Supporting Information

for

Evaluation of nanostructured β-$Mn_2V_2O_7$ thin films as photoanodes for photoelectrochemical water oxidation

Yash Gargasya[1], Melissa K. Gish[2], Vineet V. Nair[3], Justin C. Johnson[2] and Matt Law[1,3]

[1]Department of Chemistry, University of California, Irvine, CA 92617, USA
[2]National Renewable Energy Laboratory, Golden, CO 80401, USA
[3]Department of Chemical Engineering and Materials Science, University of California, Irvine, CA 92617, USA

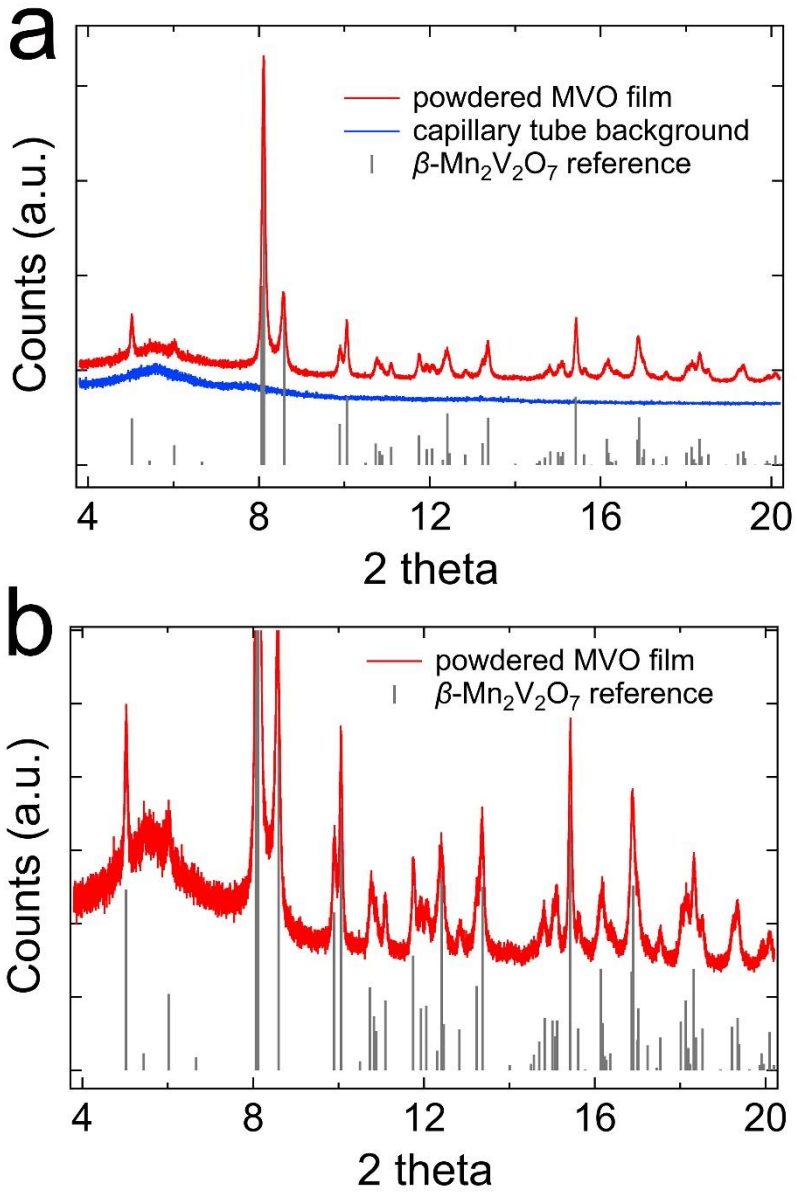

Figure S1. High-resolution synchrotron powder XRD of a powderized β-MVO film. The film was 580 nm thick, made on FTO-coated glass substrates using a 30 minute calcination at 500 °C (a "standard" film). λ = 0.458092 Å. All peaks index to β-MVO (grey bars).

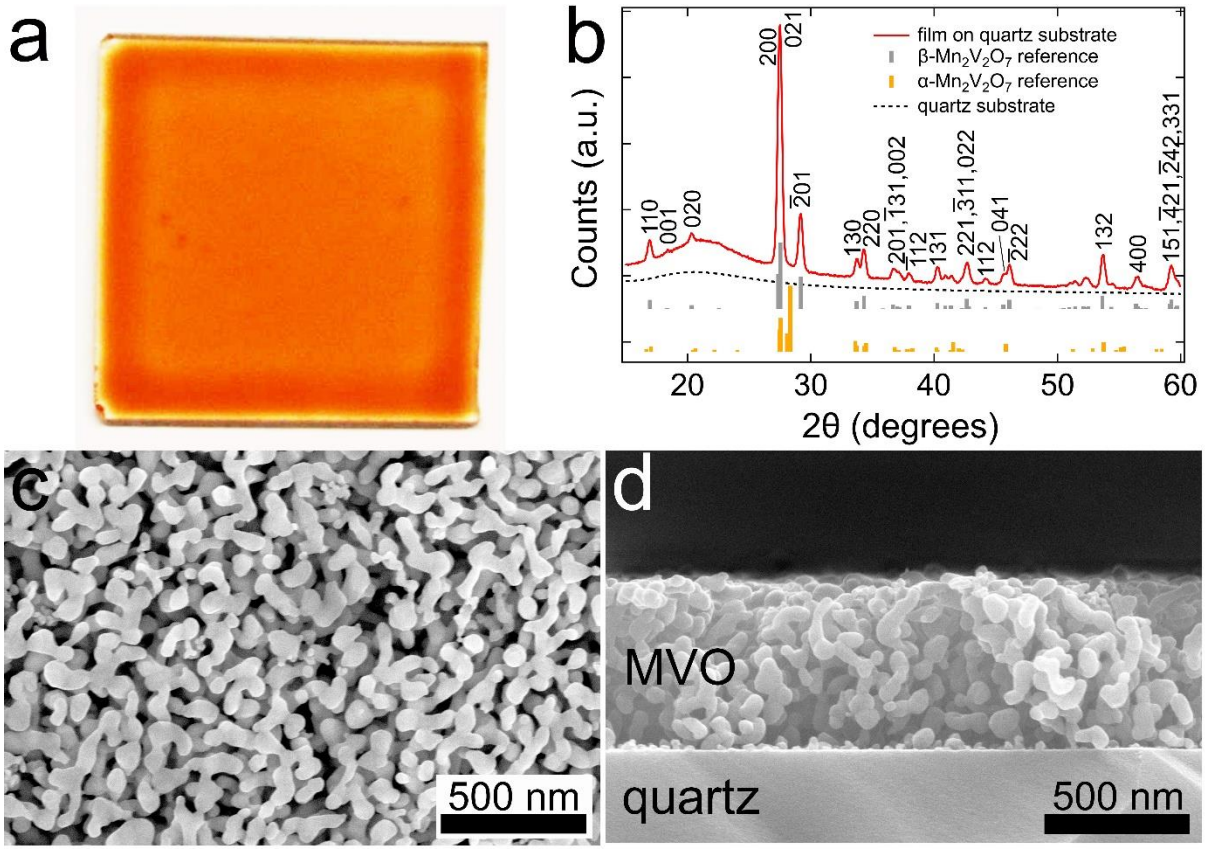

Figure S2. Characterization of nanostructured MVO films on quartz substrates. (a) Photograph of a 570 ± 35 nm thick MVO film on a 1×1 inch quartz substrate. (b) XRD pattern of a duplicate film. All peaks index to β-$Mn_2V_2O_7$ (PDF# 01-089-0484, grey bars) and the sample appears to be phase pure. The broad peak at 23° is due to the quartz substrate. (c-d) Plan view and cross-section SEM images of the film.

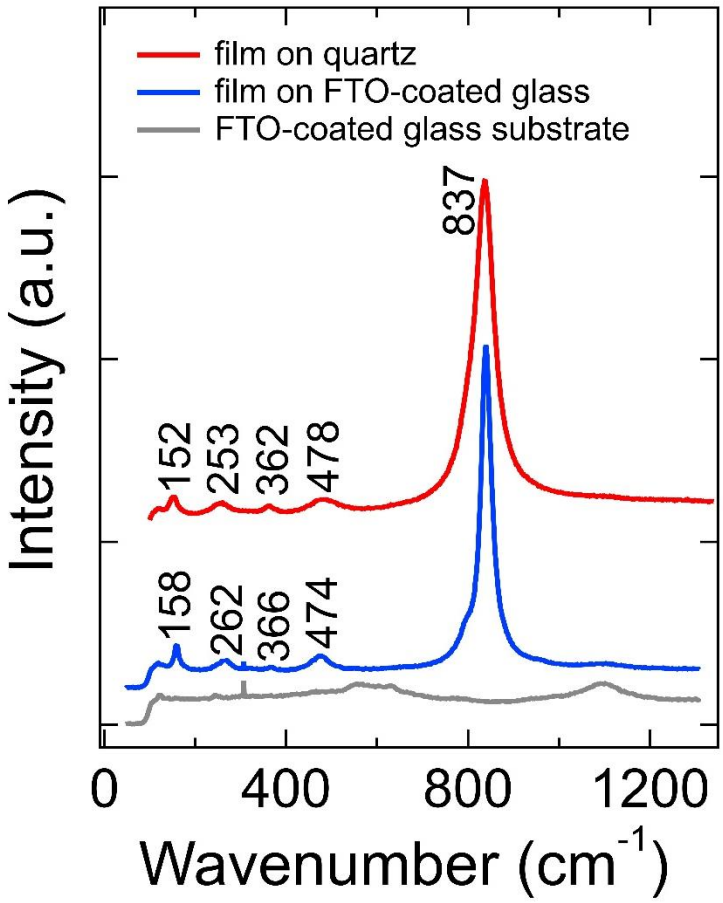

Figure S3. Raman spectra of β-MVO films on FTO-coated glass and quartz substrates. The spectrum of a bare FTO-coated glass substrate is also shown.

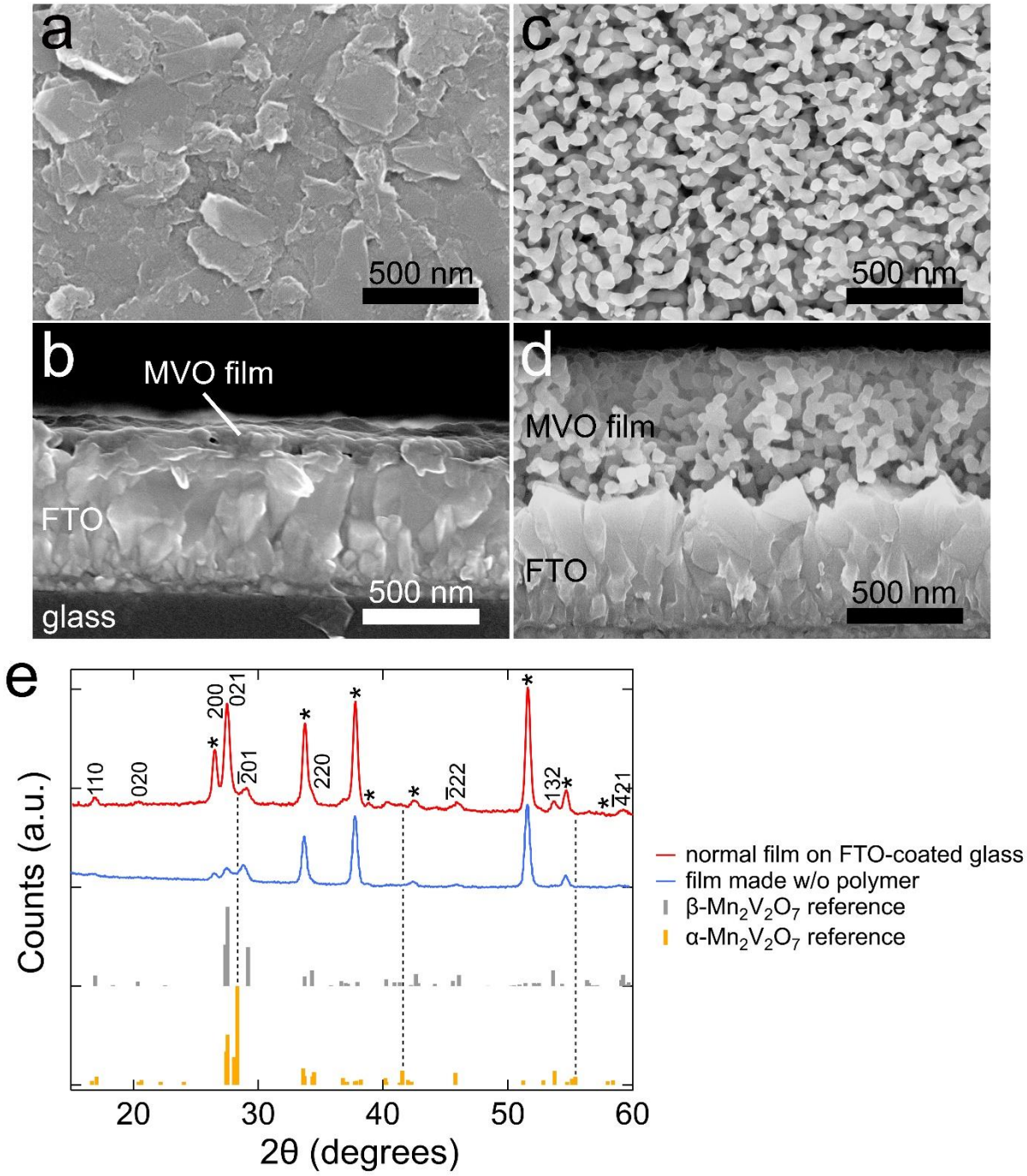

Figure S4. Characterization of a representative MVO film made without the Pluronic F-108 triblock copolymer. (a-b) Plan view and cross-section SEM images of an MVO film made without the polymer. The film is nonporous and thin. The substrate is FTO-coated glass. (c-d) Corresponding SEM images of a standard β-MVO film. (e) XRD patterns of the two films. Reference patterns for β-MVO (gray bars) and α-MVO (orange bars) are also shown.

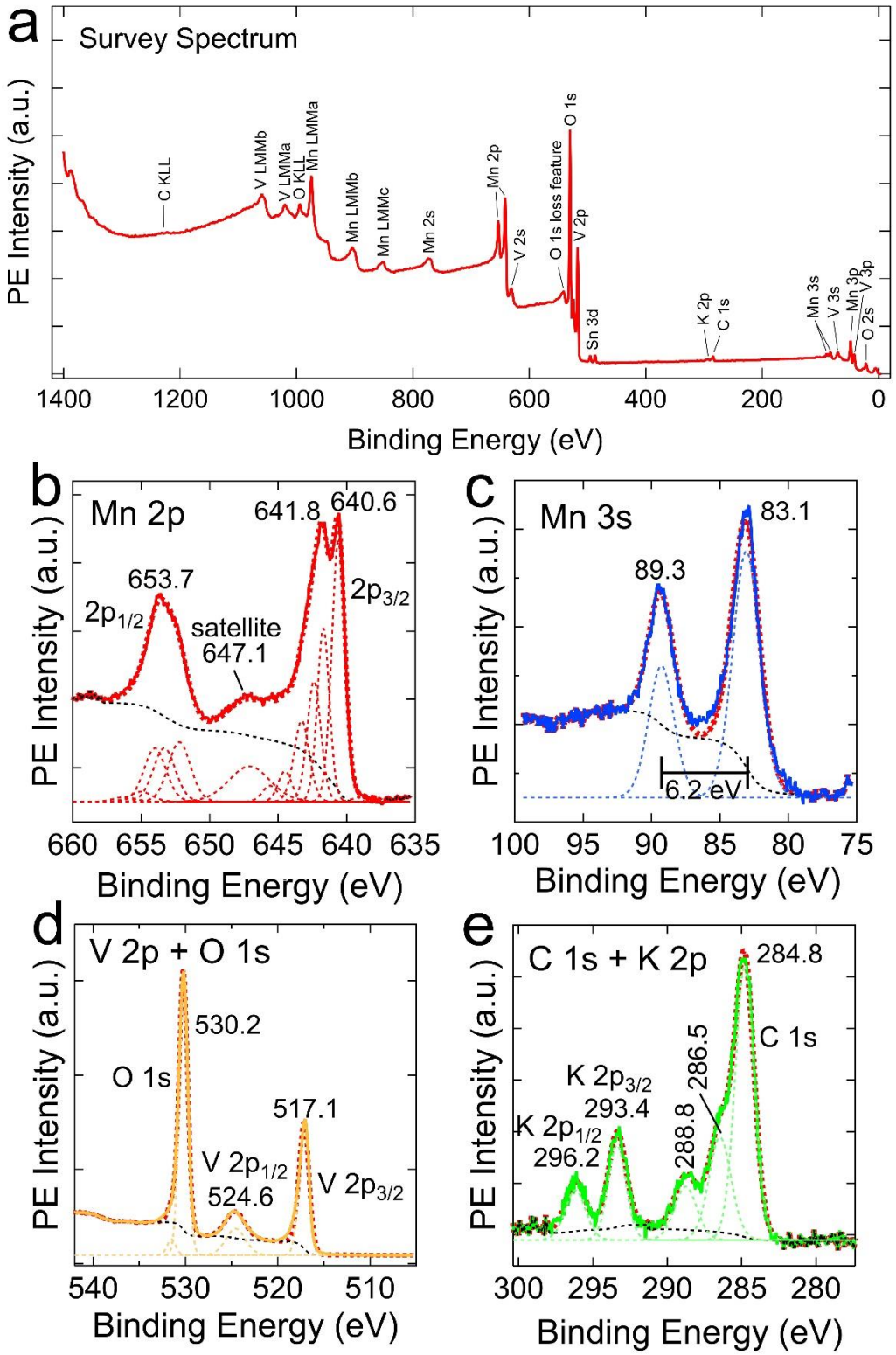

Figure S5. XPS analysis of a standard *β*-MVO film on an FTO-coated glass substrate. (a) Indexed survey scan. The only elements detected were Mn, V, O, C, K (origin unknown), and Sn (from the substrate). (b) Mn 2p region. (c) Mn 3s region. (d) V 2p and O 1s region. (e) C 1s and K 2p region. Each high-resolution spectrum shows the raw data (solid lines), background (dashed black line), peaks (colored dashed lines), and sum (heavy dashed red line). A Mn:V atomic ratio of 1.09 was measured for this sample (see Table 2).

Table S1. Ink composition and fabrication conditions for the different MVO films.

Film Thickness/ Grain Size (nm)	Mn (mmol)	V (mmol)	HNO_3 (g)	H_2O/EG (g)	F-108 (g)	Annealing		Spin Speed / Time (rpm / sec)
						Temp (°C)	Time (min)	
260/61	1	1	0.32	1.5/1.5	0.4	500	30	5000 / 20 6000 / 40
575/64	1	1	0.32	1.5/1.5	0.4	500	30	2000 / 20 3000 / 40
1000/61	1	1	0.32	1.0/1.0	0.4	500	30	2000 / 20 3000 / 40
3200/66	1	1	0.32	0.5/0.5	0.4	500	30	1500 / 20 2200 / 40
4650/66	1	1	0.32	0.5/0.5	0.4	500	30	750 / 20 1200 / 40
557/39	1	1	0.32	1.5/1.5	0.4	500	15	2000 / 20 3000 / 40
537/89	1	1	0.32	1.5/1.5	0.4	500	60	2000 / 20 3000 / 40
570/110	1	1	0.32	1.5/1.5	0.4	500	120	2000 / 20 3000 / 40

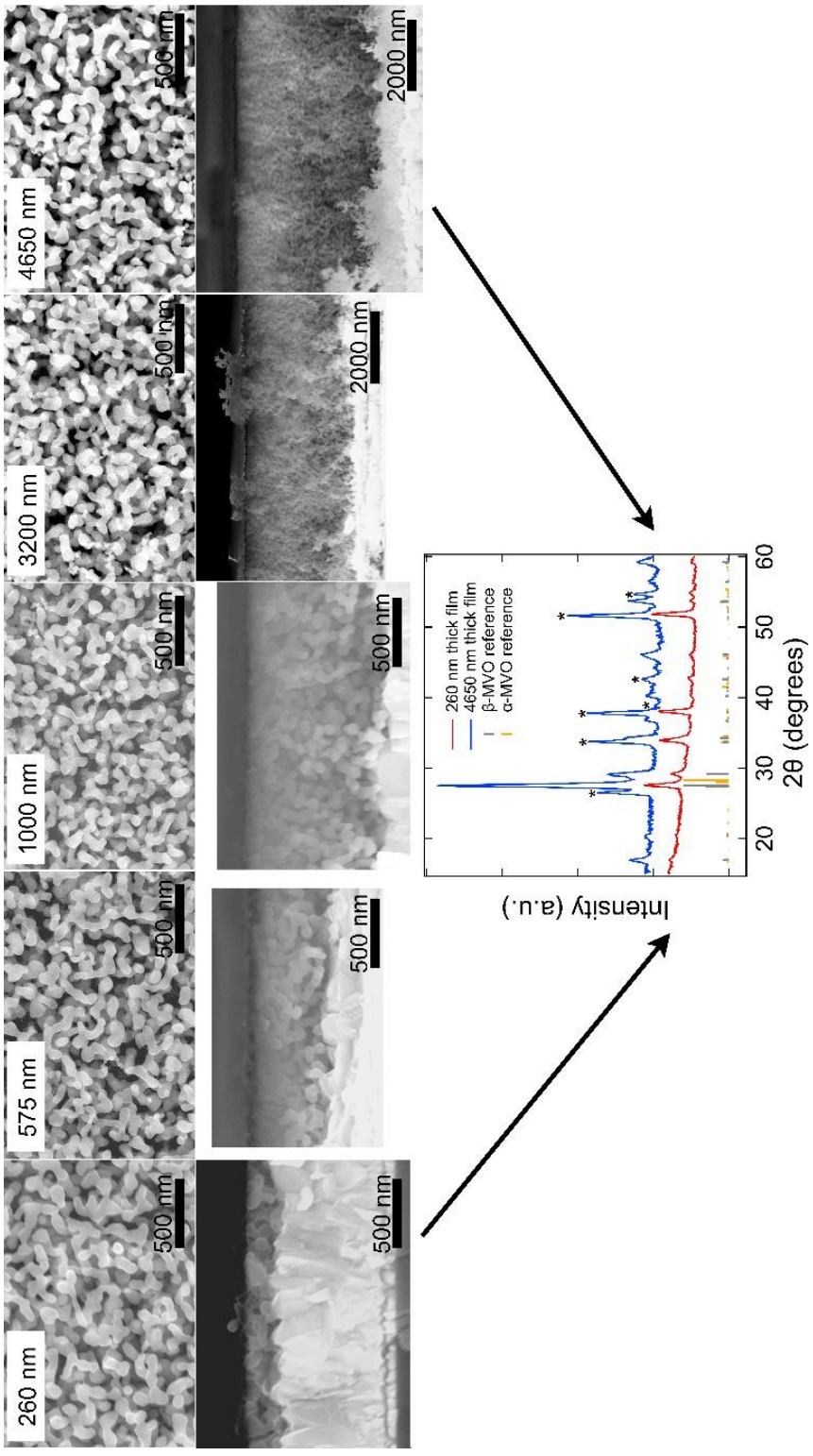

Figure S6. *β*-MVO films of different thickness. (*top*) Plan view and cross-section SEM images of films with a thickness of 260, 575, 1000, 3200, and 4650 nm. All films have an average crystallite diameter of 55-65 nm and were grown on FTO-coated glass substrates. (*bottom*) Grazing-incidence XRD patterns of the thinnest and thickest films (red and blue traces, respectively). Both films are phase-pure *β*-MVO. Asterisks denote substrate peaks. Reference patterns for *β*-MVO (gray bars) and *α*-MVO (orange bars) are also shown. The angle of incidence was 0.2° and 1.5° for the 260 and 4650 nm thick films, respectively. Film thickness was tuned by changing the solvent volume and spin coating parameters (Table S1).

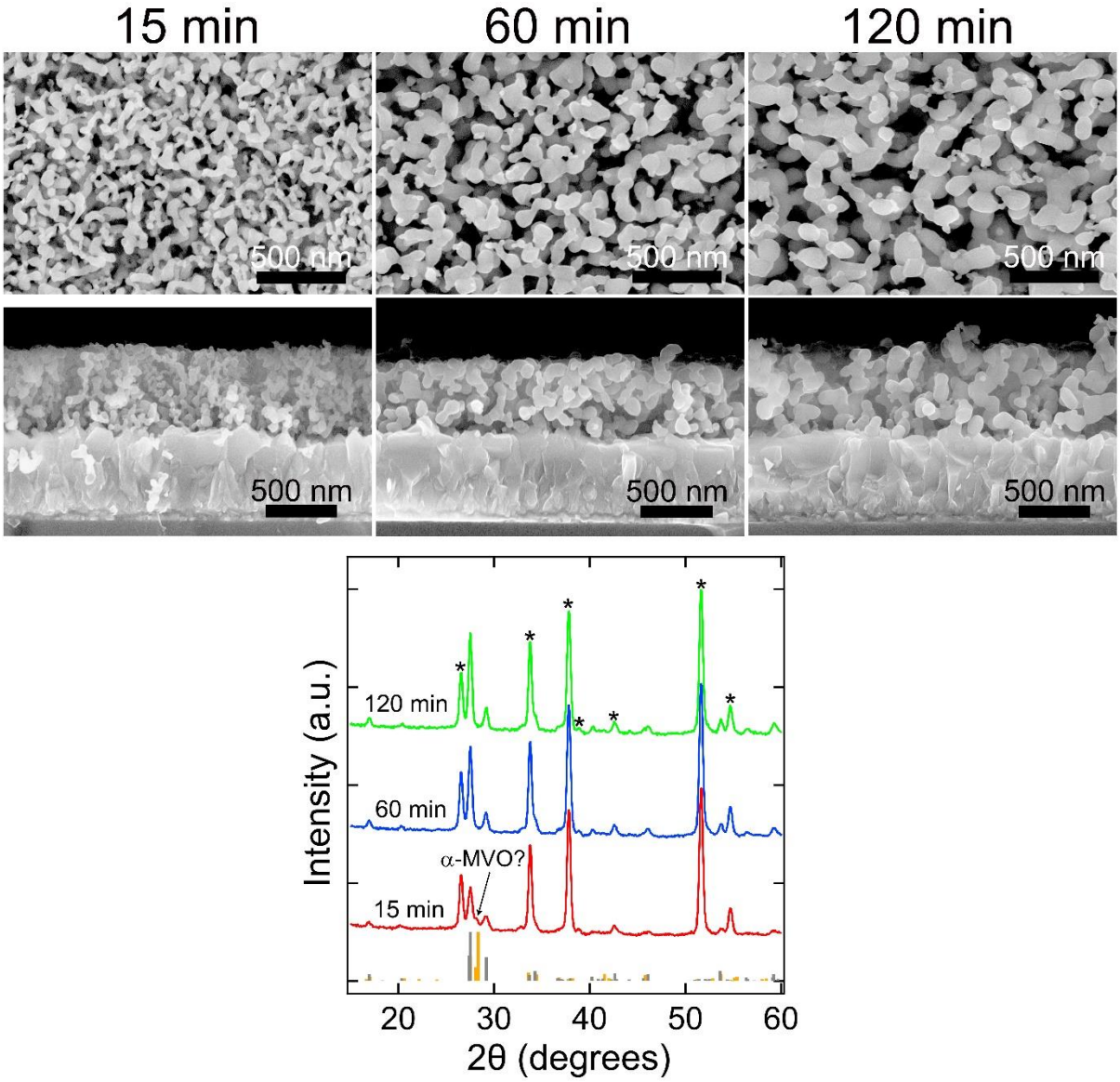

Figure S7. *β*-MVO films with different crystallite size. (*top*) Plan view and cross-section SEM images of films calcined at 500 ºC for either 15, 60, or 120 minutes, resulting in an average crystallite diameter of ~39 nm, ~89 nm, and ~110 nm, respectively. The films have a thickness of 520-580 nm and were made from a single sample deposited on an FTO-coated glass substrate and then diced into three pieces prior to calcination. (*bottom*) XRD patterns of the three films. All films are phase-pure *β*-MVO except for a small shoulder at ~28.2º in the 15-min calcined film that may be due to *α*-MVO (labelled in the figure). Asterisks denote substrate peaks. Reference patterns for *β*-MVO (gray bars) and *α*-MVO (orange bars) are also shown.

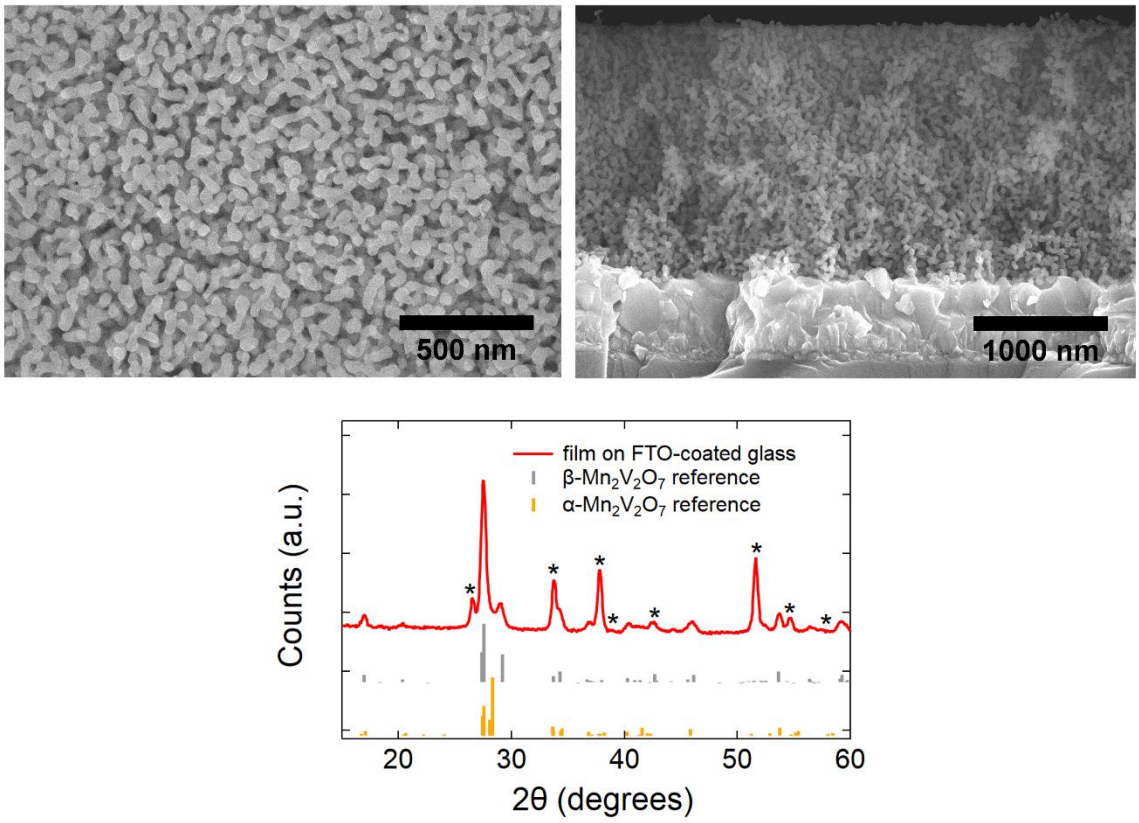

Figure S8. Characterization of an β-MVO film made using an annealing temperature and time of 475 °C and 15 minutes on an FTO-coated glass substrate. The grain size determined by SEM is 28.8 nm ± 6.7 nm.

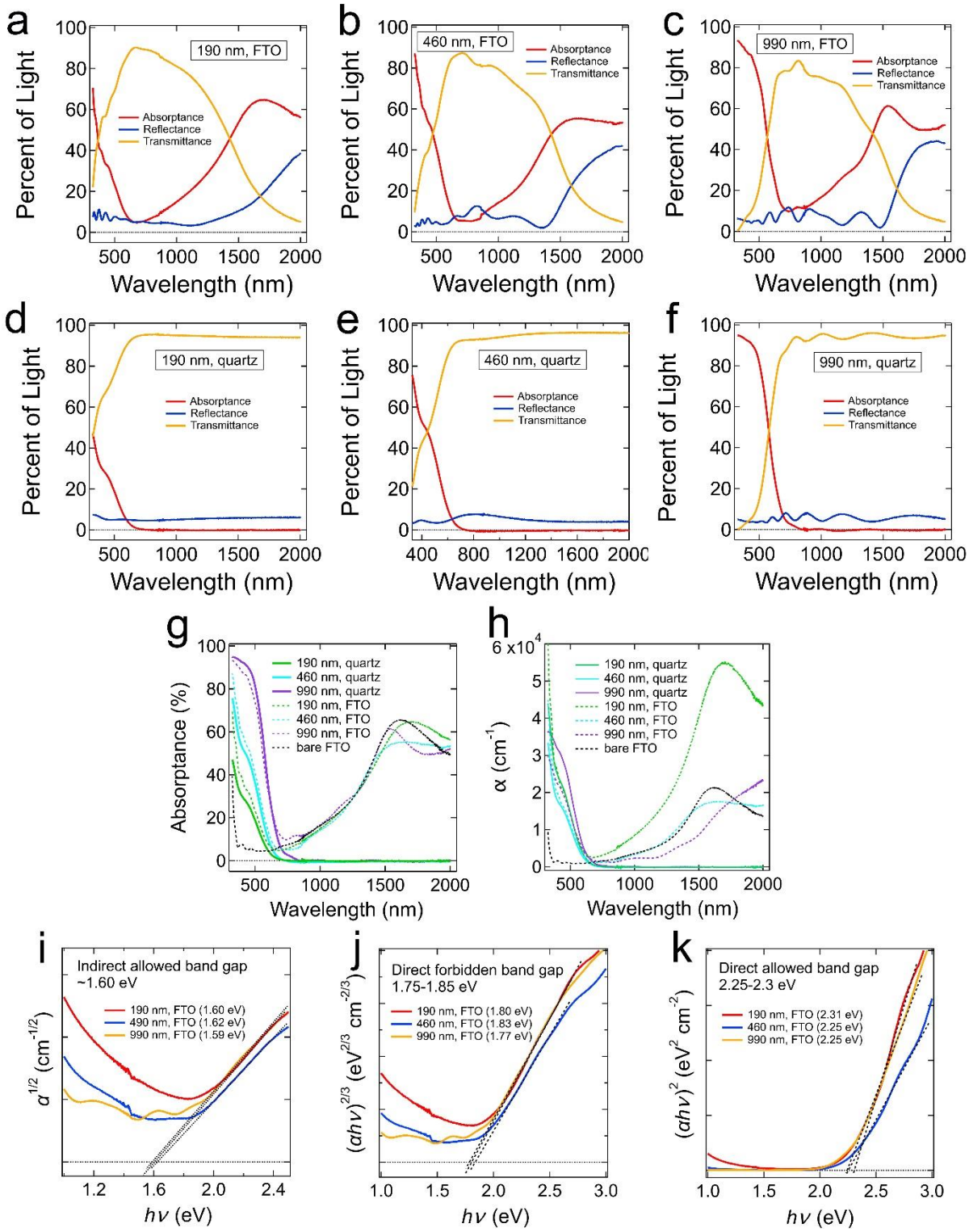

Figure S9. (a-f) Absorptance, reflectance, and transmittance spectra of MVO films of various thickness grown on FTO-coated glass and quartz substrates. (g) Compiled absorptance spectra of these samples. The spectrum of a bare FTO-coated glass substrate is also shown for reference. Figure S9 shows the full data for the bare substrate. (h) Absorptivity spectra of the samples and the bare FTO-coated glass substrate. The absorptivity of the MVO samples was calculated using only the MVO film thickness, without including the thickness of the FTO layer. The absorptivity of the bare FTO substrate was calculated using the thickness of the FTO layer (~500 nm). (i-k) Fitted Tauc plots for the MVO films on FTO-coated glass substrates.

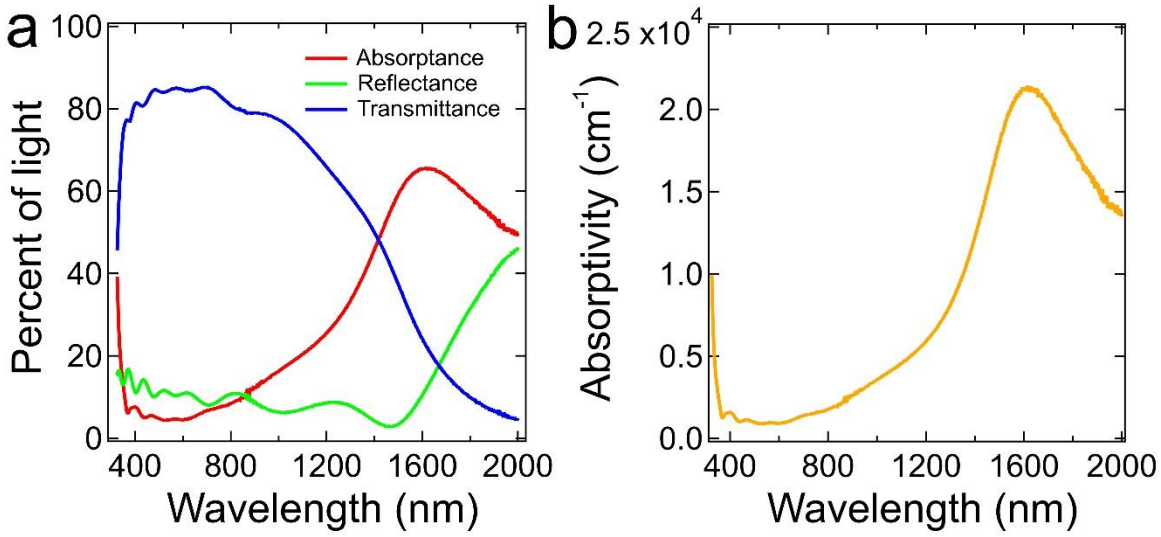

Figure S10. (a) Measured transmittance, reflectance, and absorptance spectra and (b) absorptivity spectrum of a clean FTO-coated glass substrate.

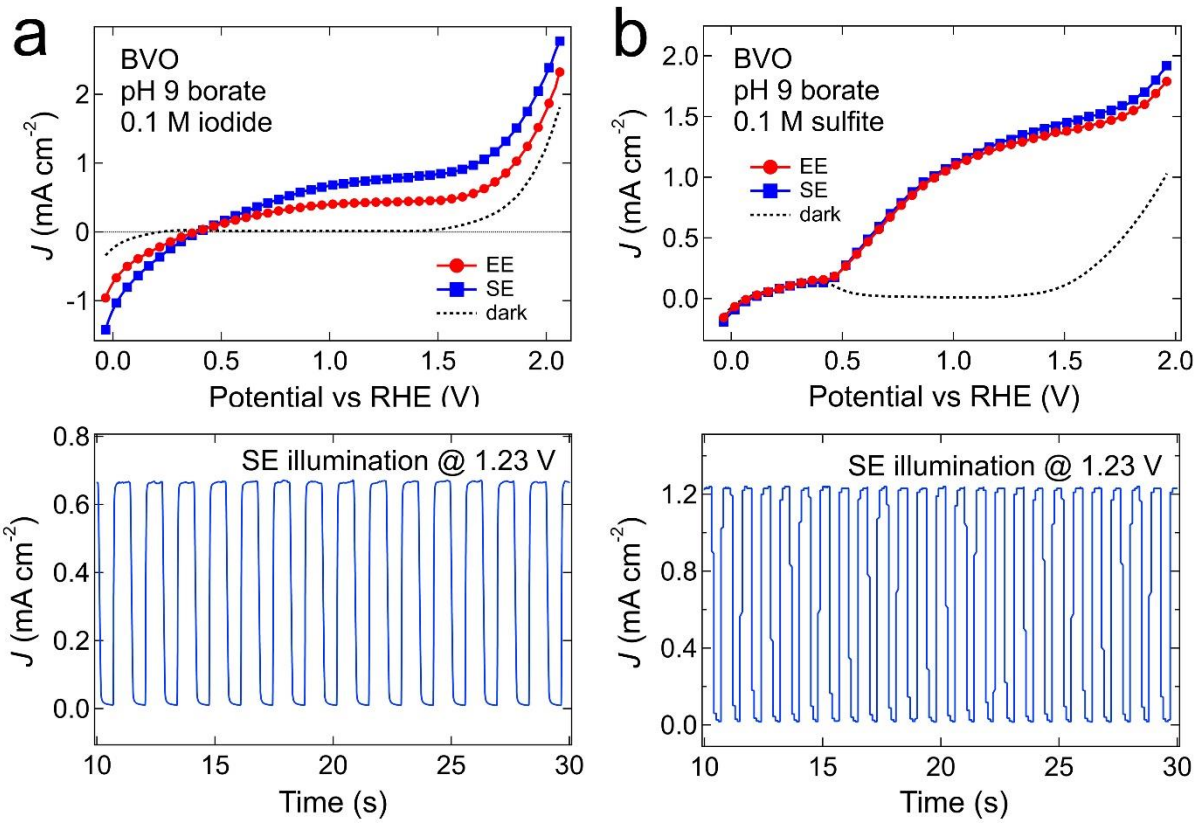

Figure S11. Photoelectrochemical *J-E* and *J-t* data for $BiVO_4$ (BVO) films measured in 0.1 M aqueous borate buffer (pH 9) with (a) 0.1 M potassium iodide and (b) 0.1 M sodium sulfite as a hole scavenger. The *J-t* data were acquired at 1.23 V vs. RHE using chopped illumination (1.25 Hz) in the SE geometry.

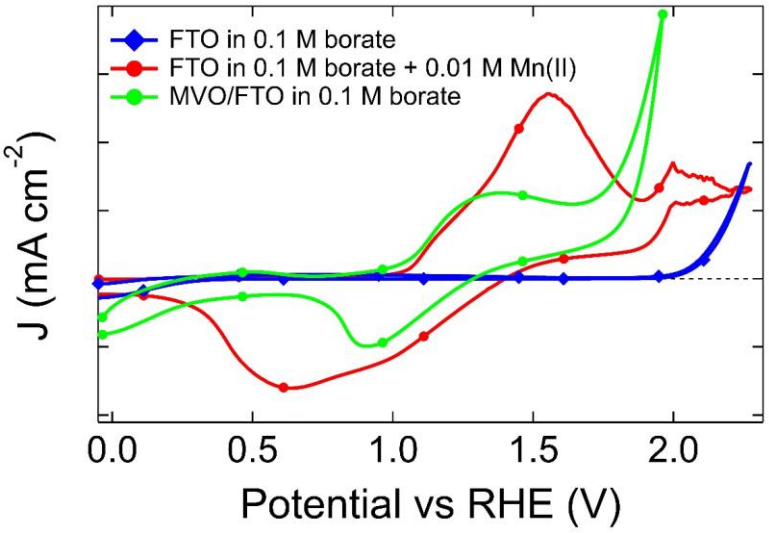

Figure S12. Cyclic voltammetry (CV) data for a blank FTO-coated glass substrate in a 10 mM solution of Mn(II) acetate in 0.1 M borate buffer at pH 9 (*red*) shows a reversible redox wave around the same potentials as observed in scans of MVO films in pure 0.1 M borate buffer at pH 9 (*green*). This reversible redox wave is assigned to the Mn^{3+}/Mn^{2+} couple, which is known to have a standard reduction potential of 1.5 V vs. RHE at 25 ºC. The oxidation wave at 1.3-1.5 V for the MVO films is believed to result from the oxidation of both Mn^{2+} ions in the electrolyte and surface manganese on the films. Exact potentials can differ depending on the chemical environment of the Mn and the presence of other ions in the solutions that act as ligands and shift the redox potentials. The presence of a variety of Mn species (dissolved and surface) may explain the broadness of the peaks. Note that CV scans of V^{5+} solutions showed no peaks in this region.

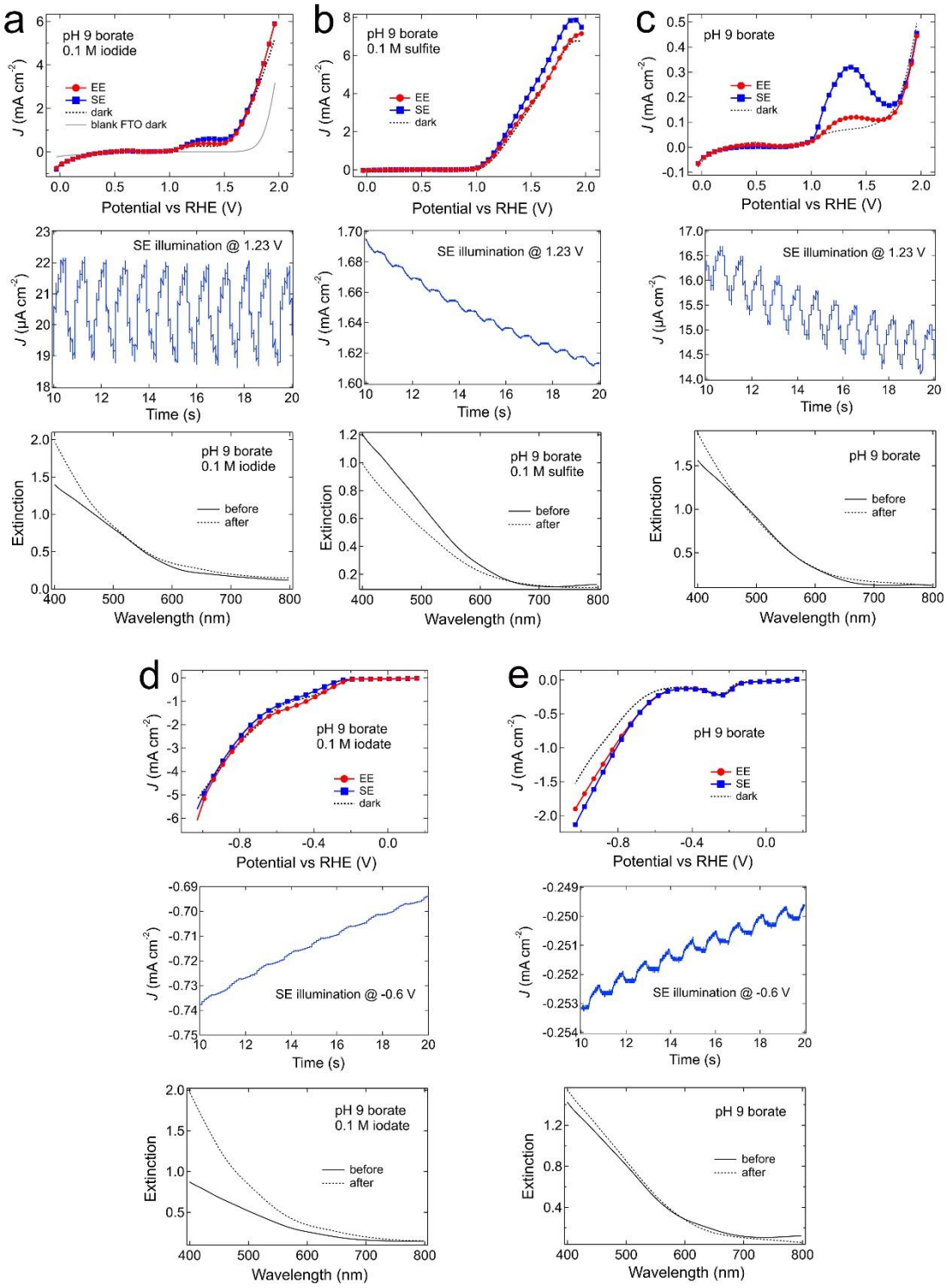

Figure S13. Photoelectrochemical (PEC) data for MVO films in 0.1 M aqueous borate buffer at pH 9. Current-potential (*J-E*) and current-time (*J-t*) plots and optical extinction spectra immediately before and after PEC measurements for (a) iodide oxidation, (b) sulfite oxidation, (c) water oxidation, (d) iodate reduction, and (e) water reduction. *J-E* data were acquired at a potential sweep rate of 50 mV/s. *J-t* data were acquired at either 1.23 V vs. RHE (for oxidations) or -0.6 V vs. RHE (for reductions) using chopped illumination (1.25 Hz) in the SE geometry. PEC data required ~20 minutes to collect per sample, so Δt ~ 20 minutes for each set of optical spectra. All of the MVO films were 580 ± 60 nm thick except for the film tested in iodate, which was ~450 nm thick. See Methods for other details.

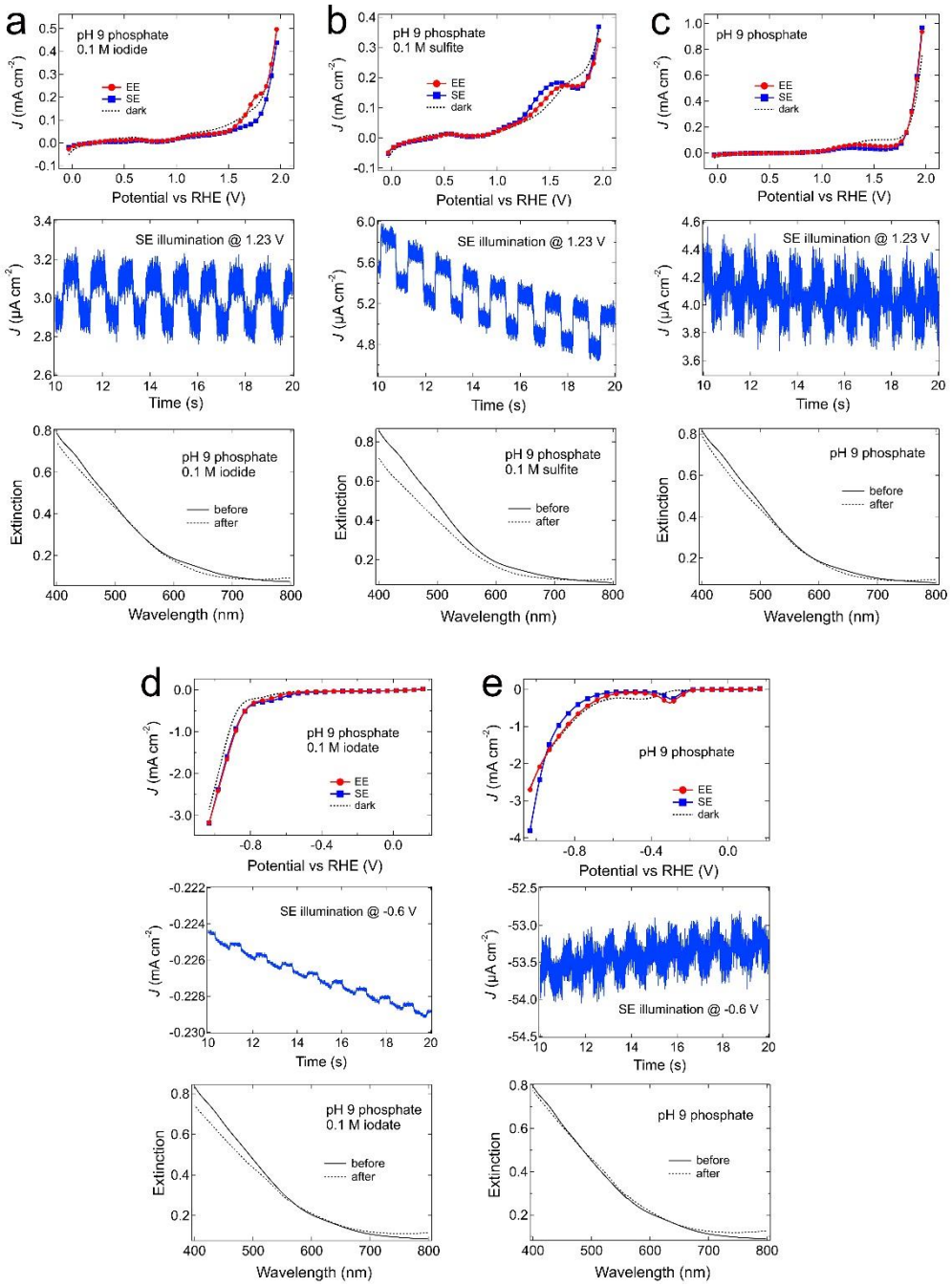

Figure S14. Photoelectrochemical (PEC) data for MVO films in 0.1 M aqueous phosphate buffer at pH 9. Current-potential (*J-E*) and current-time (*J-t*) plots and optical extinction spectra immediately before and after PEC measurements for (a) iodide oxidation, (b) sulfite oxidation, (c) water oxidation, (d) iodate reduction, and (e) water reduction. *J-E* data were acquired at a potential sweep rate of 50 mV/s. *J-t* data were acquired at either 1.23 V vs. RHE (for oxidations) or -0.6 V vs. RHE (for reductions) using chopped illumination (1.25 Hz) in the SE geometry. PEC data required ~20 minutes to collect per sample, so Δt ~ 20 minutes for each set of optical spectra. All of the MVO films were 400 ± 60 nm thick. See Methods for other details.

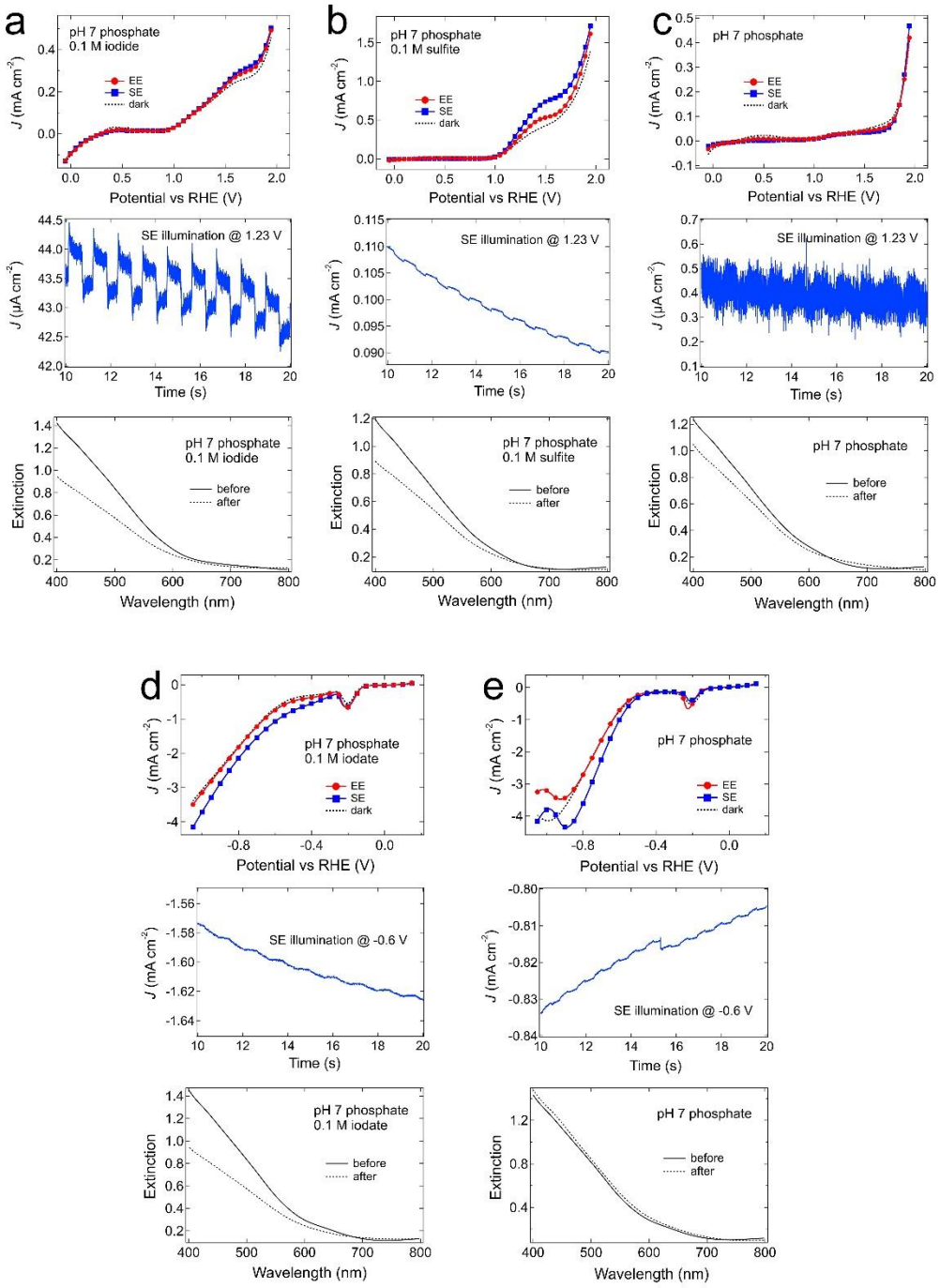

Figure S15. Photoelectrochemical data for MVO films in 0.1 M aqueous phosphate buffer at pH 7. Current-potential (*J-E*) and current-time (*J-t*) plots and optical extinction spectra immediately before and after PEC measurements for (a) iodide oxidation, (b) sulfite oxidation, (c) water oxidation, (d) iodate reduction, and (e) water reduction. *J-E* data were acquired at a potential sweep rate of 50 mV/s. *J-t* data were acquired at either 1.23 V vs. RHE (for oxidations) or -0.6 V vs. RHE (for reductions) using chopped illumination (1.25 Hz) in the SE geometry. PEC data required ~20 minutes to collect per sample, so Δt ~ 20 minutes for each set of optical spectra. All of the MVO films were 580 ± 60 nm thick. See Methods for other details.

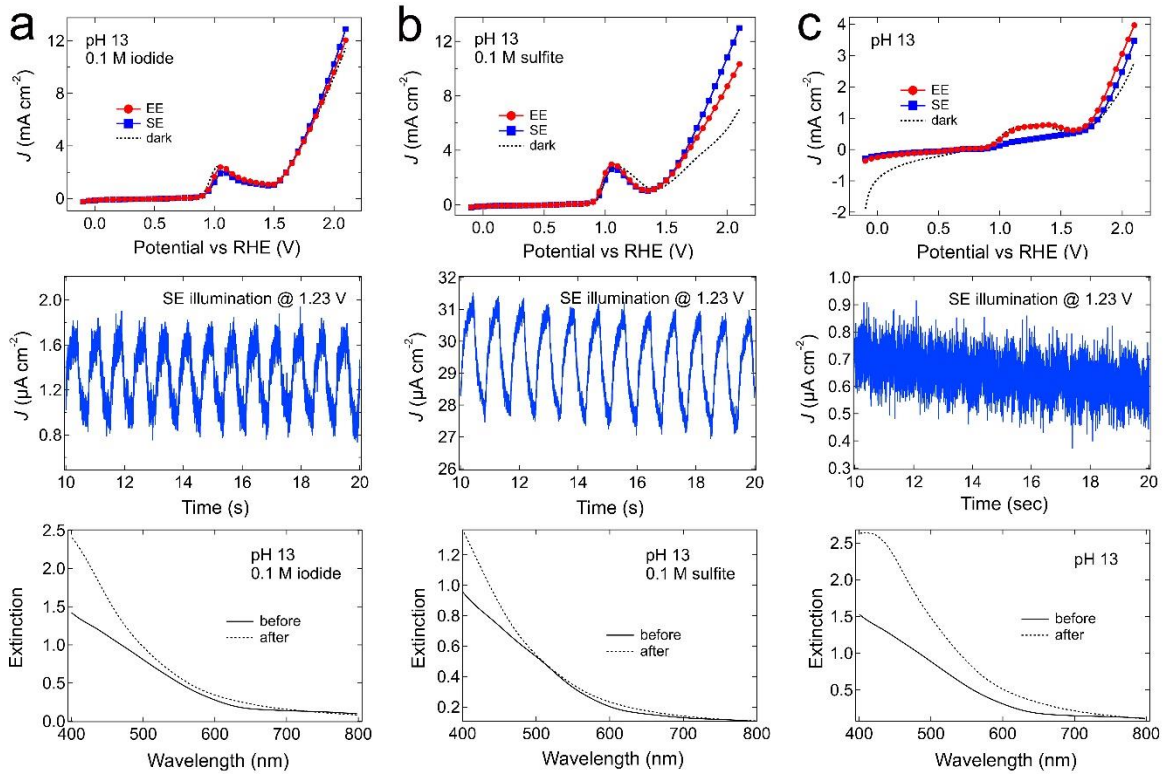

Figure S16. Photoelectrochemical data for MVO films in 0.1 M aqueous NaOH solution (pH 13). Current-potential (*J-E*) and current-time (*J-t*) plots and optical extinction spectra immediately before and after PEC measurements for (a) iodide oxidation, (b) sulfite oxidation, and (c) water oxidation. *J-E* data were acquired at a potential sweep rate of 50 mV/s. *J-t* data were acquired at 1.23 V vs. RHE using chopped illumination (1.25 Hz) in the SE geometry. PEC data required ~20 minutes to collect per sample, so $\Delta t \sim 20$ minutes for each set of optical spectra. All of the MVO films were 580 ± 60 nm thick except for the film tested in iodate, which was ~480 nm thick. See Methods for other details.

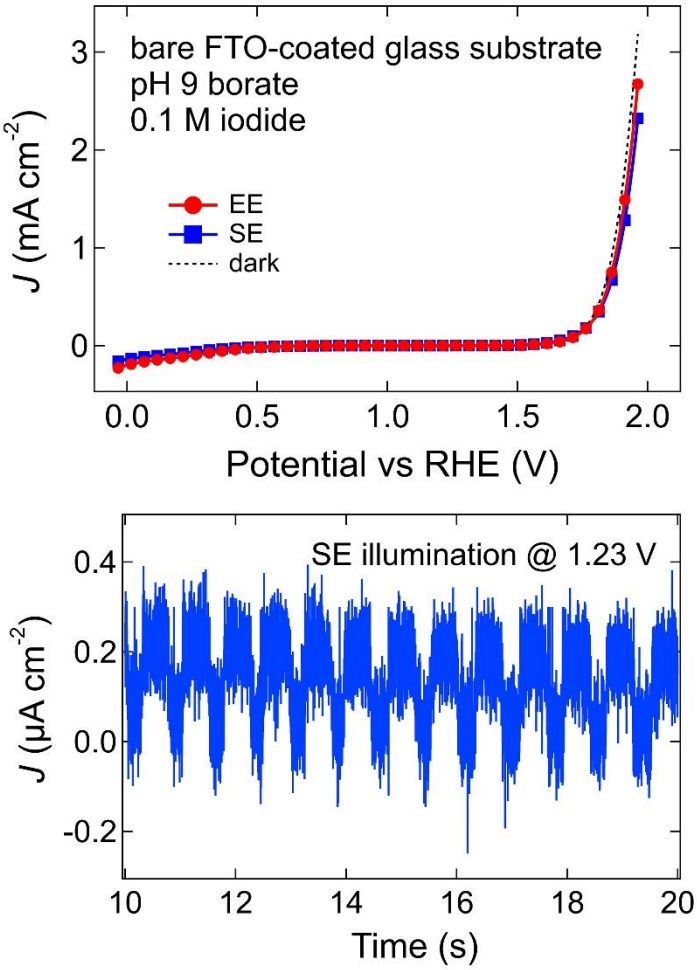

Figure S17. Photoelectrochemical data for a blank FTO-coated glass substrate (no MVO film) in 0.1 M aqueous borate buffer containing 0.1 M iodide at pH 9. *J-E* data were acquired at a potential sweep rate of 50 mV/s. *J-t* data were acquired at 1.23 V vs. RHE using chopped illumination (1.25 Hz) in the SE geometry. The "photocurrent" was only ~0.3 µA cm^{-2}. See Methods for experimental details.

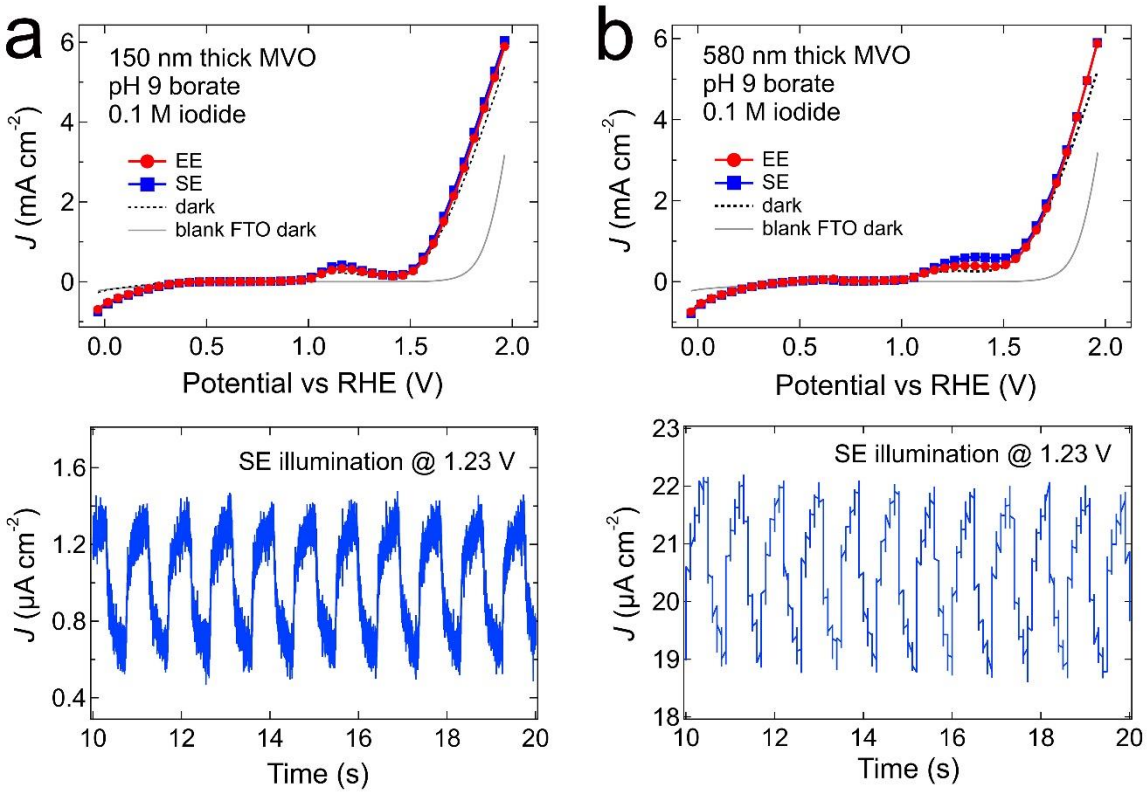

Figure S18. Photoelectrochemical (PEC) data for MVO films of different thickness. Current-potential (*J-E*) and current-time (*J-t*) data for iodide oxidation in pH 9 borate buffer for films with a thickness of (a) 150 nm and (b) 580 nm. *J-E* data were acquired at a potential sweep rate of 50 mV/s. *J-t* data were acquired at 1.23 V vs. RHE using chopped illumination (1.25 Hz) in the SE geometry. See Methods for other details.

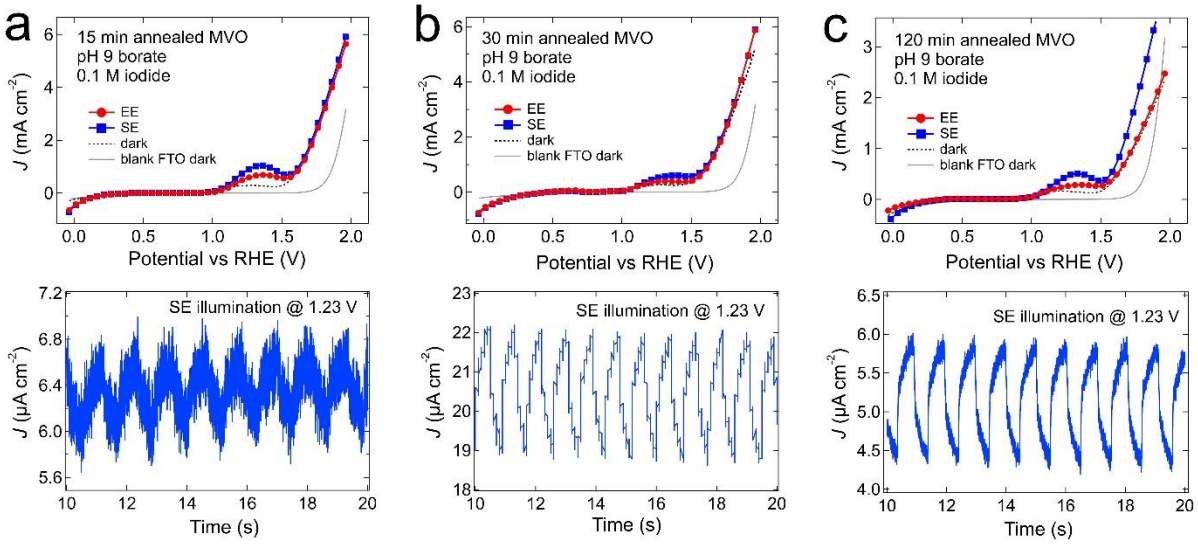

Figure S19. Photoelectrochemical (PEC) data for MVO films as a function of MVO annealing time. Current-potential (*J-E*) and current-time (*J-t*) data for iodide oxidation in pH 9 borate buffer for films annealed at 500 ºC for (a) 15 minutes, (b) 30 minutes, and (c) 120 minutes. *J-E* data were acquired at a potential sweep rate of 50 mV/s. *J-t* data were acquired at 1.23 V vs. RHE using chopped illumination (1.25 Hz) in the SE geometry. All of the MVO films were 580 ± 60 nm thick. See Methods for other details.

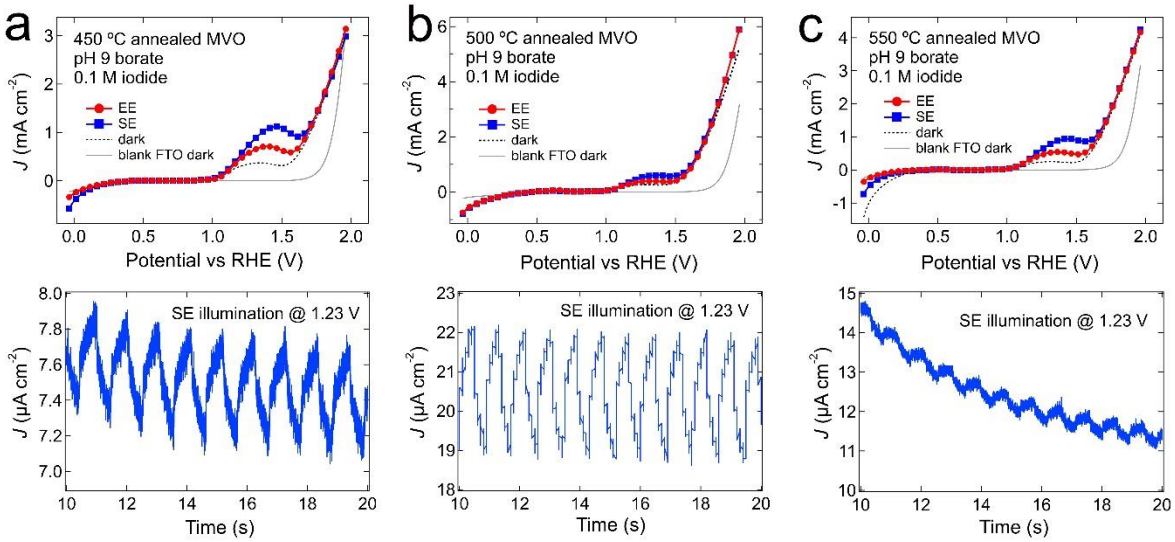

Figure S20. Photoelectrochemical (PEC) data for MVO films as a function of MVO annealing temperature. Current-potential (*J-E*) and current-time (*J-t*) data for iodide oxidation in pH 9 borate buffer for films annealed at (a) 450 ºC, (b) 500 ºC, and (c) 550 ºC for 30 minutes. *J-E* data were acquired at a potential sweep rate of 50 mV/s. *J-t* data were acquired at 1.23 V vs. RHE using chopped illumination (1.25 Hz) in the SE geometry. All of the MVO films were 580 ± 60 nm thick. See Methods for other details.

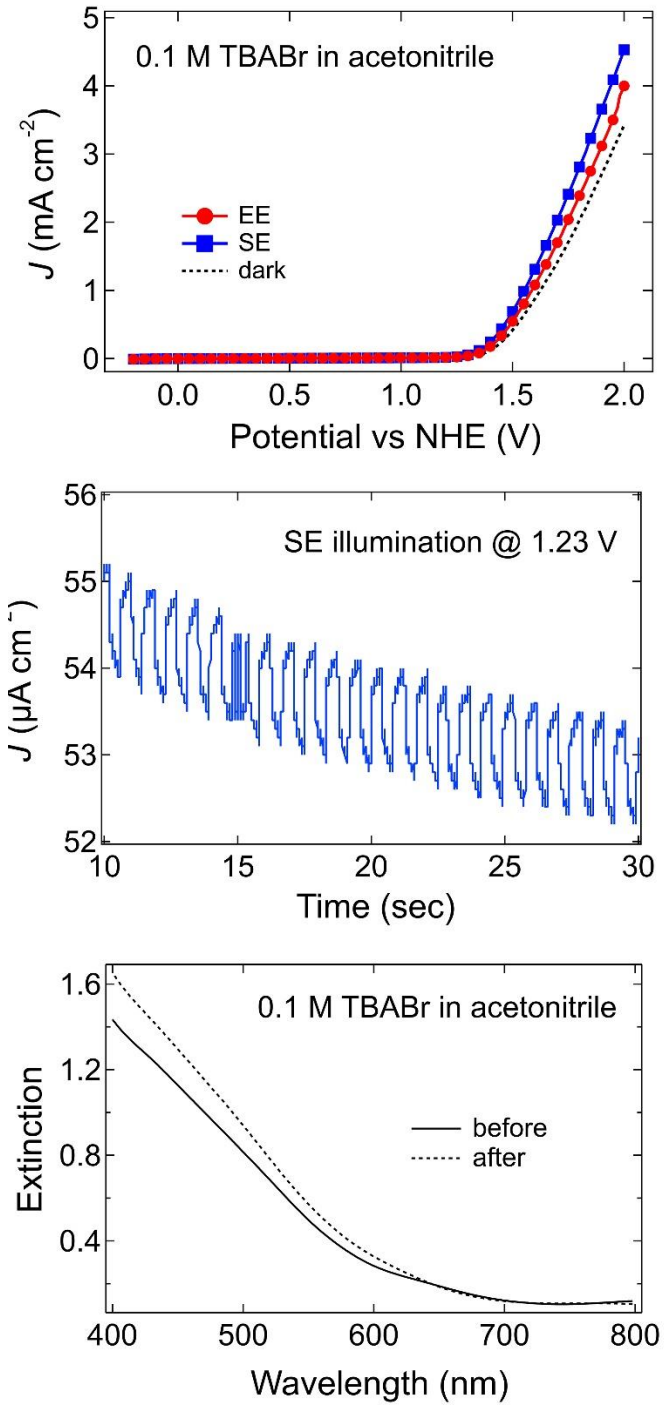

Figure S21. Non-aqueous photoelectrochemical data for an MVO film in 0.1 M tetrabutylammonium bromide (TBABr) in dry acetonitrile. Current-potential (*J-E*), current-time (*J-t*), and optical extinction spectra immediately before and after PEC measurements for bromide oxidation. *J-E* data were acquired at a potential sweep rate of 50 mV/s. *J-t* data were acquired at 1.23 V vs. NHE using chopped illumination (1.25 Hz) in the SE geometry. PEC data required ~20 minutes to collect per sample, so Δt ~ 20 minutes for the two optical spectra. The MVO film was 580 ± 60 nm thick. See Methods for other details.

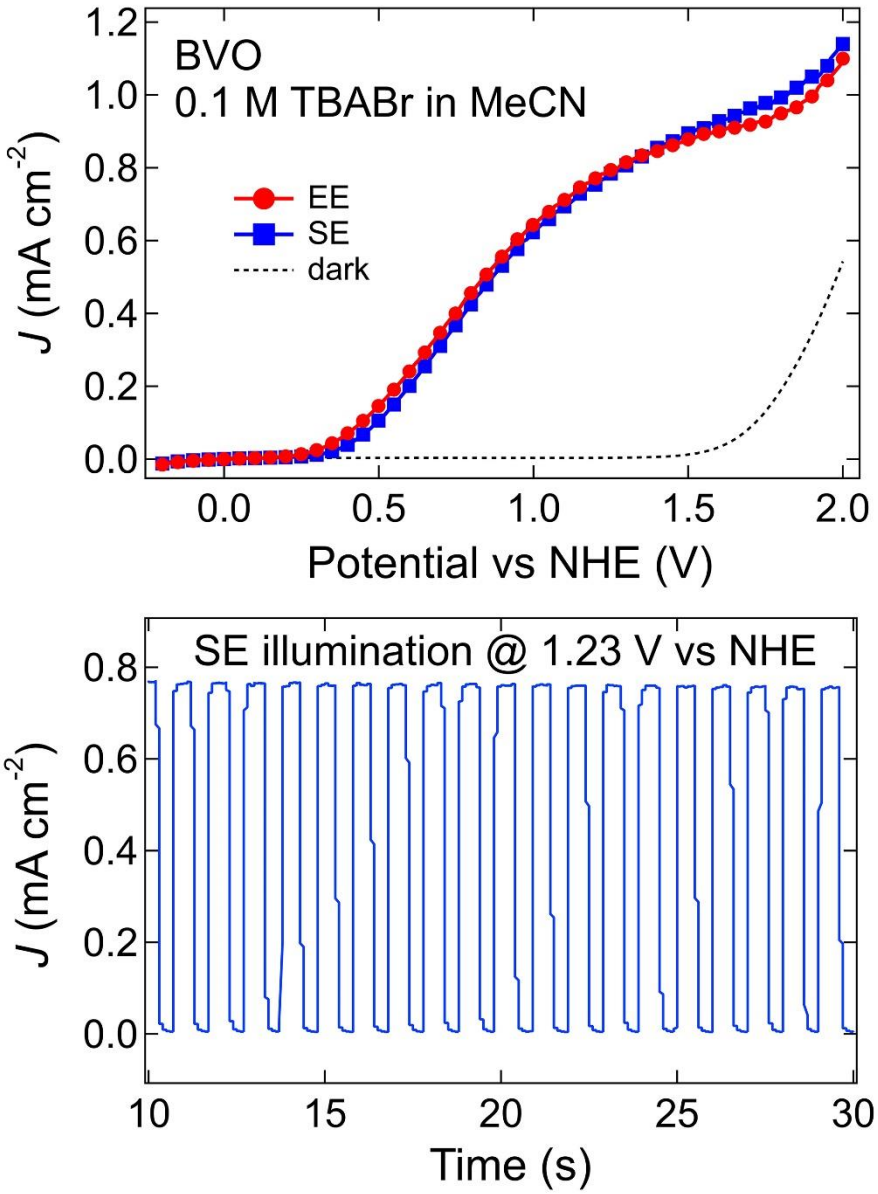

Figure S22. Photoelectrochemical *J-E* and *J-t* data for a $BiVO_4$ (BVO) film measured in 0.1 M tetrabutylammonium bromide in acetonitrile. A photocurrent of ~0.75 mA cm^{-2} was measured at 1.23 V vs. NHE (1 Sun AM1.5G illumination). The *J-t* data were acquired at 1.23 V vs. NHE using chopped illumination (1.25 Hz) in the SE geometry.

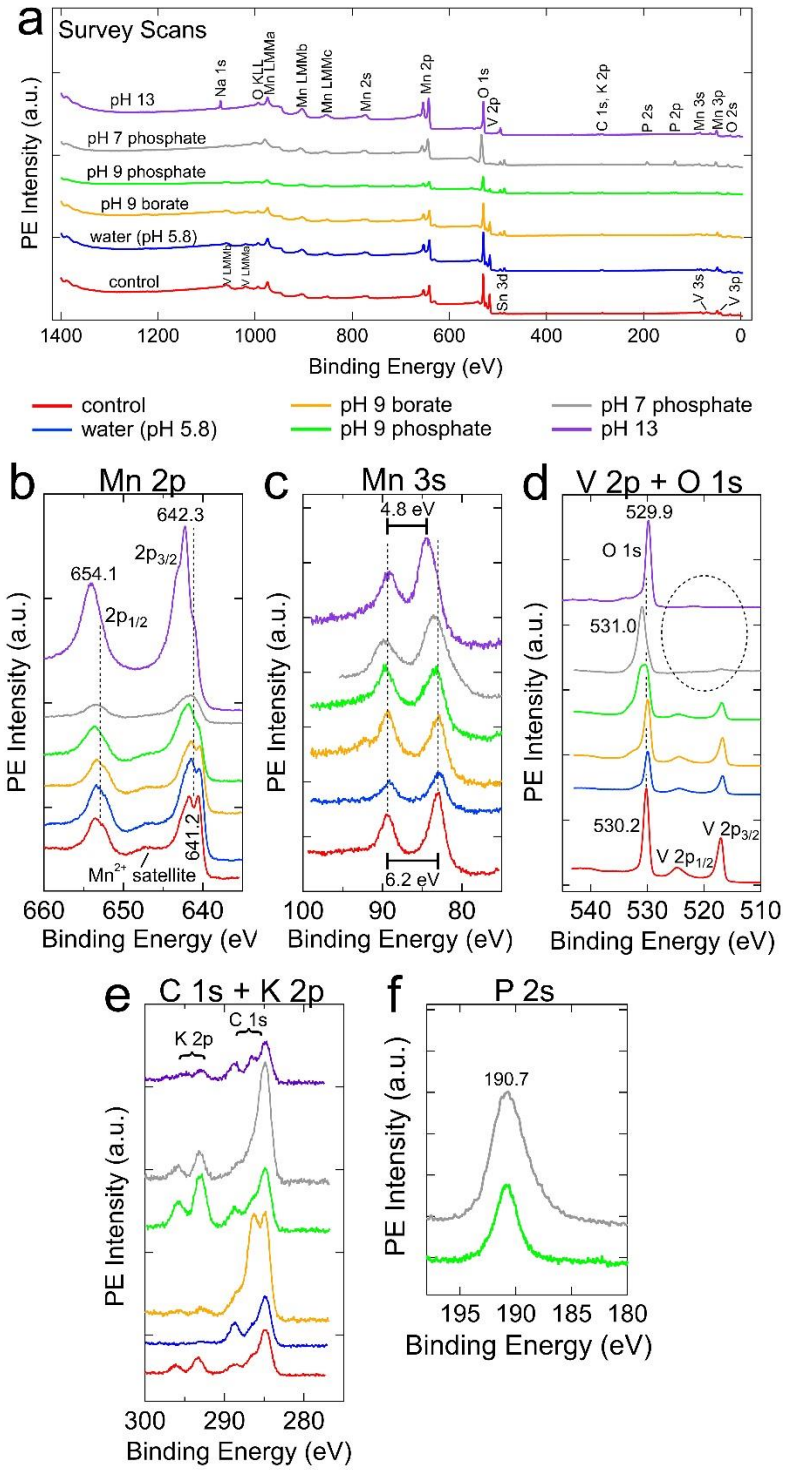

Figure S23. XPS data for standard β-MVO films immersed in various aqueous solutions for 20 hours unbiased in the dark. The solutions did not contain added Mn or V species. (a) Indexed survey scans. The only elements detected were Mn, V, O, C, K (origin unknown), Sn (from the substrate), P in the two films immersed in phosphate buffer, and Na on the film aged in 0.1 M NaOH. (b) Mn 2p region. The films aged in pure water (pH 5.8) and 0.1 M borate solution at pH 9 have nearly the same spectrum as the dry control film. The film aged in 0.1 M phosphate solution at pH 9 shows the appearance of higher-energy $2p_{3/2}$ and $2p_{1/2}$ peaks consistent with partial conversion of Mn^{2+} to Mn^{3+}, possibly in the form of amorphous Mn_2O_3, Mn_3O_4, and/or Mn(III)-containing phosphates.[1,2,3] The film aged in 0.1 M phosphate solution at pH 7 appears

to contain mostly Mn^{3+}, but broadening of the Mn 3s peaks (see below) suggests that substantial Mn^{2+} is still present. Finally, the spectrum of the film treated in 0.1 M NaOH (pH 13) is characteristic of Mn^{4+}, which is mostly likely present in the form of amorphous $MnO(OH)_2$ and MnO_2. (c) Mn 3s region. The energy separation between the two multiplet-split components decreases from 6.2 eV (characteristic of Mn^{2+}) for the control film to 4.8 eV (characteristic of Mn^{4+}) for the film aged at pH 13.[4] There is also substantial peak broadening in the film aged in pH 7 phosphate solution that is consistent with the presence of both Mn^{3+} and Mn^{2+}. (d) V 2p and O 1s region. The O 1s spectrum of the control film features a strong, narrow peak originating from the lattice oxygen of MVO. There is also a very weak high-energy tail probably caused by surface hydroxides. This tail becomes a small shoulder at ~532 eV in the film aged in water. The shoulder is more prominent for the film treated in borate solution. Immersion in pH 9 phosphate solution results in the appearance of an O 1s peak at 531 eV due to PO_4^{3-}.[5] Both phosphate and metal oxide lattice oxygen are present in this sample, as is the high-energy shoulder. Meanwhile, the vanadium peaks are significantly reduced in intensity, consistent with partial loss of vanadium and formation of Mn phosphates. The film aged in pH 7 phosphate solution exhibits a single oxygen peak at 531.0 eV due to phosphate. The metal oxide peak is largely gone. The high-energy shoulder is still present but weaker. Furthermore, the vanadium signal is almost gone (dashed oval). This is consistent with extensive conversion of the sample to Mn phosphates. Aging at pH 13 causes loss of all vanadium signal and a sharp oxygen peak at 529.9 eV with weak high-energy features that we assign to the bulk oxygen of MnO_2 plus surface hydroxides. (e) C 1s and K 2p region. (f) P 2s region. The binding energy of 190.7 eV is consistent with phosphate (PO_4^{3-}).[6] See Table 2 in the text for the Mn:V atomic ratio of each sample.

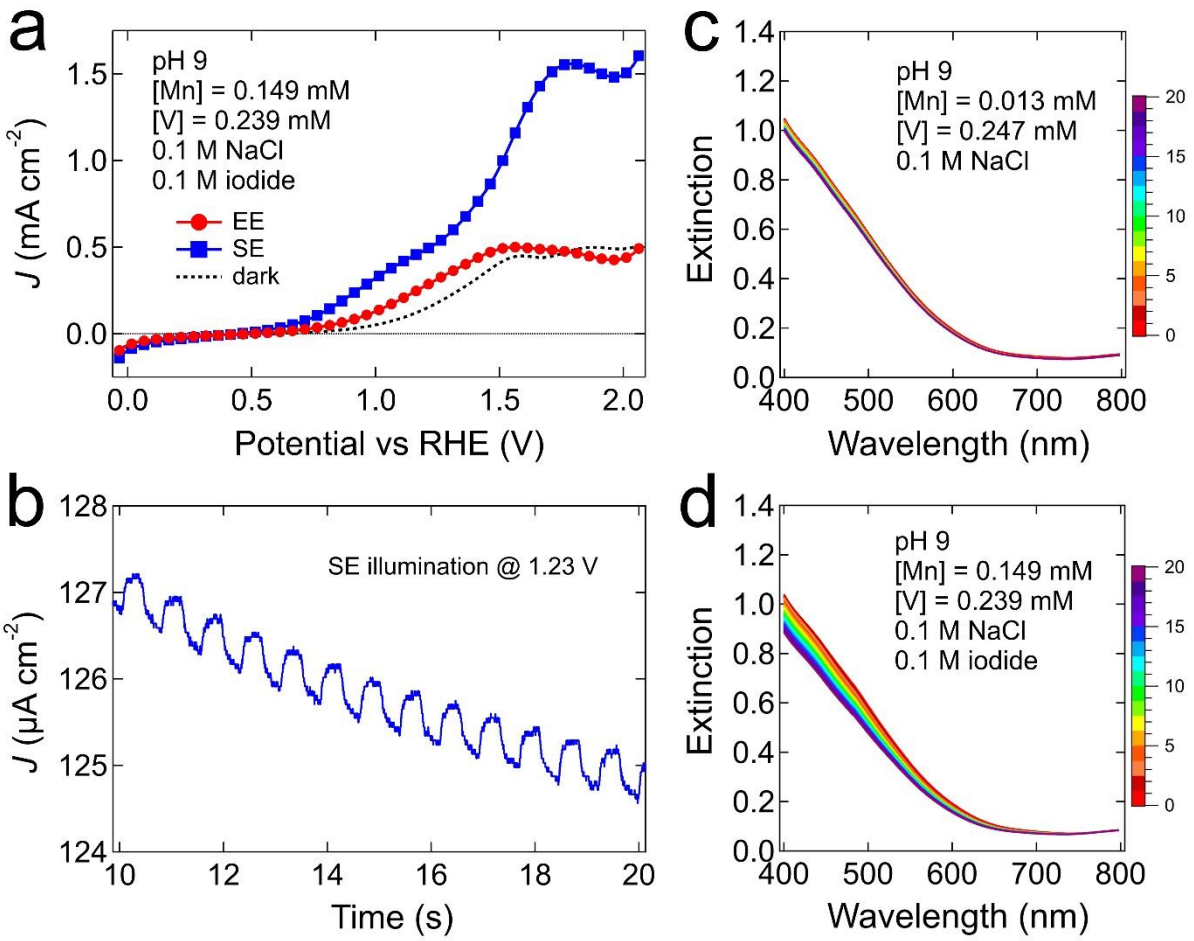

Figure S24. (a) Current-potential (*J-E*) and (b) current-time (*J-t*) plots for iodide oxidation by *β*-MVO films in Mn- and V-saturated electrolyte. The electrolyte composition was 0.149 ± 0.006 mM Mn, 0.239 ± 0.008 mM V, 0.1 M NaCl, and 0.1 M KI at pH 9. *J-E* data were acquired at a sweep rate of 50 mV/s. *J-t* data were acquired at 1.23 V vs. RHE using chopped illumination (1.25 Hz) in the SE geometry. (c) Representative spectral time series for films aged unbiased in the dark for 20 hours in 0.1 M NaCl containing 0.013 ± 0.001 mM Mn and 0.247 ± 0.009 mM V at pH 9 and (d) 0.1 M NaCl containing 0.1 M KI, 0.149 ± 0.006 mM Mn and 0.239 ± 0.008 mM V at pH 9 (the same electrolyte used in panels (a-b)). Scans were acquired every 15 minutes for 20 hours. The MVO films were 520 ± 60 nm thick. See Methods for other details.

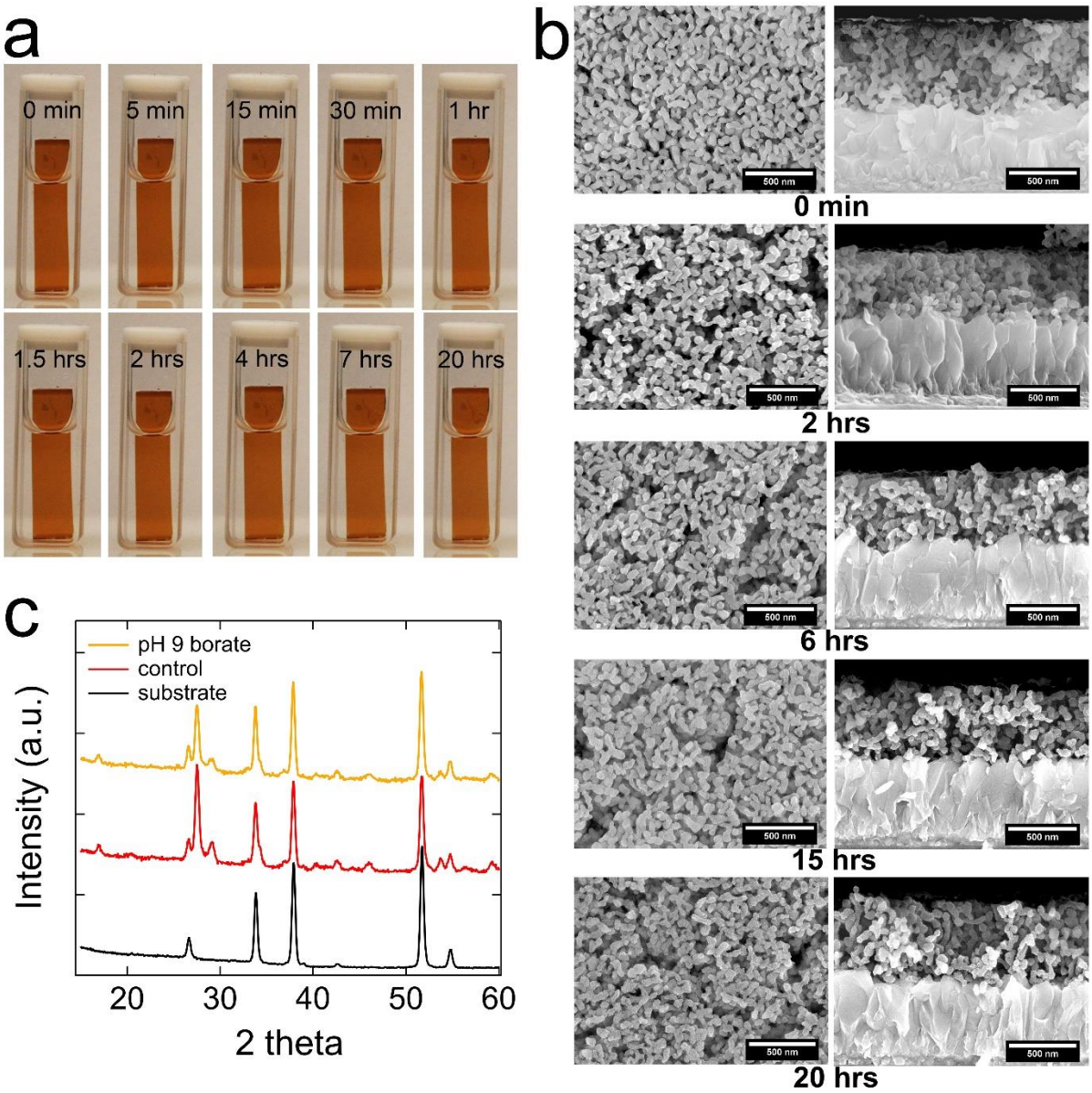

Figure S25. MVO film stability in pH 9 borate buffer solution in the absence of light and applied bias. No Mn or V was added to the initial solution. (a) Photographic time series of a film from 0 min to 20 hours of immersion in the solution. (b) Plan-view and cross-section SEM images of films aged in solution for 0 min, 2 hrs, 6 hrs, 15 hrs, and 20 hrs. Some minor surface roughening and etching of the crystallites occurs, but the gross film morphology is unchanged. (c) XRD patterns of an MVO film before immersion (red), an MVO film after 20 hrs of immersion (orange), and a clean FTO-coated glass substrate (black). The pattern of the aged film is nearly identical to that of the control film, with no new peaks.

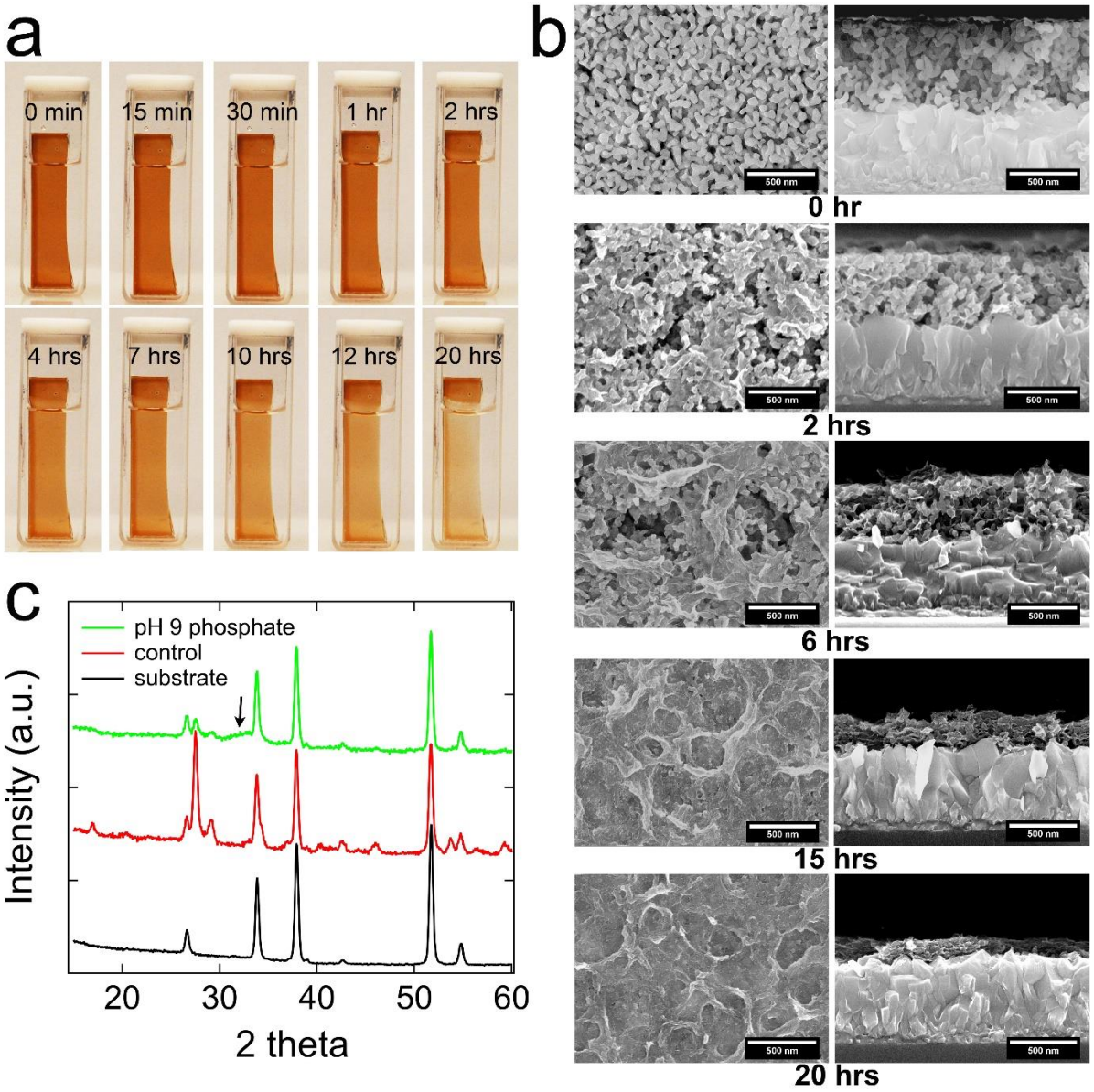

Figure S26. MVO film stability in pH 9 phosphate buffer solution in the absence of light and applied bias. No Mn or V was added to the initial solution. (a) Photographic time series of a film from 0 min to 20 hours of immersion in the solution. The color of the immersed part of the film begins to fade within several hours and becomes significantly lighter after 20 hours, consistent with partial dissolution and/or phase transformation. (b) Plan-view and cross-section SEM images of films aged in solution for 0 min, 2 hrs, 6 hrs, 15 hrs, and 20 hrs. The nanostructured film is gradually etched and slowly collapses into a dense, thinner layer within 15-20 hours. (c) XRD patterns of an MVO film before immersion (red), an MVO film after 20 hrs of immersion (green), and a clean FTO-coated glass substrate (black). The pattern of the aged film shows much smaller MVO peaks and the appearance of a weak, very broad feature at ~33 degrees (labelled with an arrow), which we assign to the 222 reflexion of α-Mn_2O_3 (PDF # 00-041-1442). Overall, these changes are qualitatively the same as in pH 7 phosphate solution, but slower.

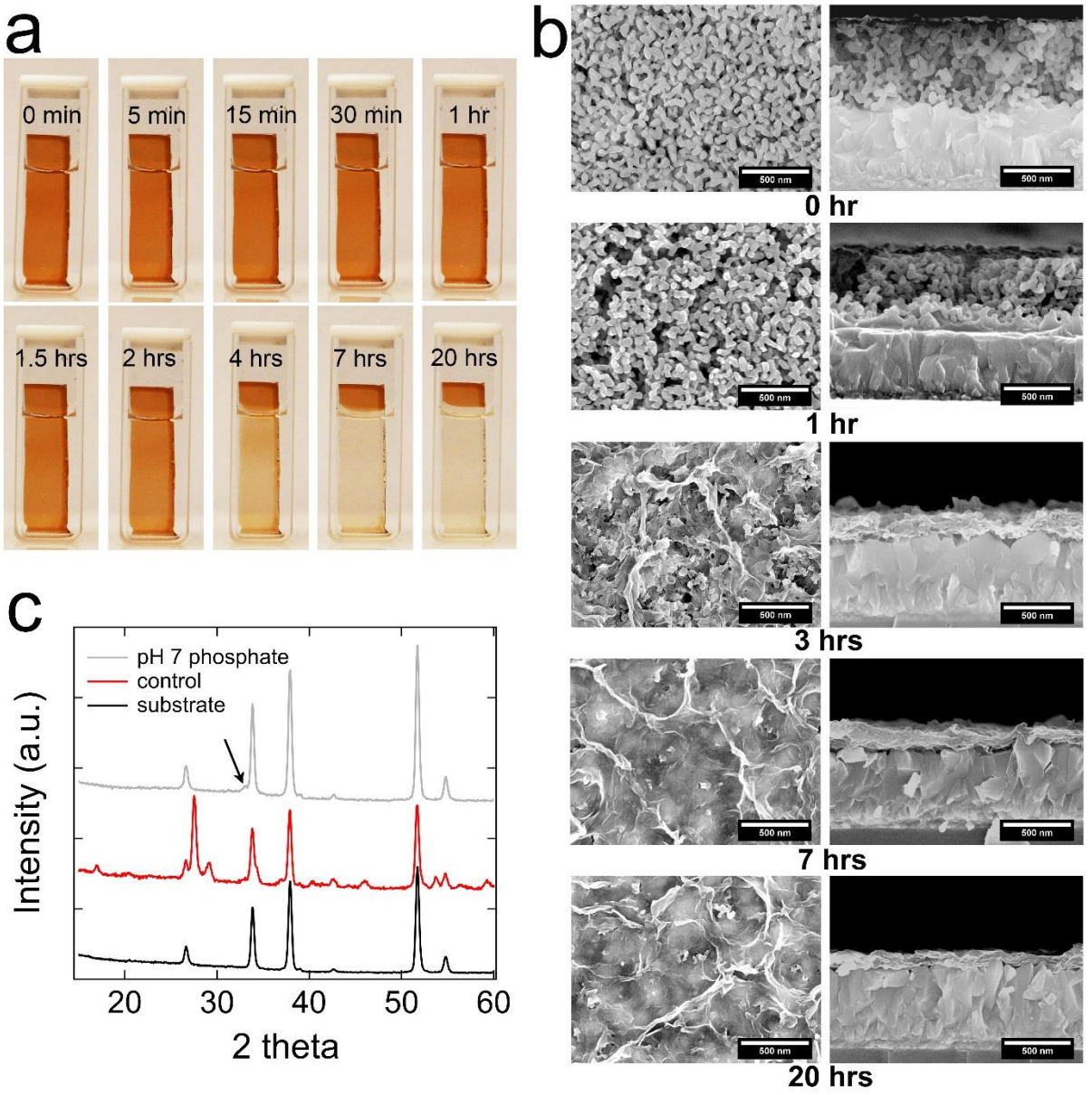

Figure S27. MVO film stability in pH 7 phosphate buffer solution in the absence of light and applied bias. No Mn or V was added to the initial solution. (a) Photographic time series of a film from 0 min to 20 hours of immersion in the solution. The color of the immersed part of the film begins to fade within 1-2 hours and becomes very faint after 20 hours, consistent with dissolution and/or phase transformation. (b) Plan-view and cross-section SEM images of films aged in solution for 0 min, 5 min, 15 min, 4 hrs, and 20 hrs. The nanostructured film collapses into a dense, much thinner layer within a few hours. This layer continues to slowly thin out to at least 20 hours. (c) XRD patterns of an MVO film before immersion (red), an MVO film after 20 hrs of immersion (gray), and a clean FTO-coated glass substrate (black). The pattern of the aged film shows a complete loss of MVO peaks and the appearance of a weak shoulder at 33.0 degrees (labelled with an arrow), which we assign to the 222 reflexion of α-Mn_2O_3 (PDF # 00-041-1442).

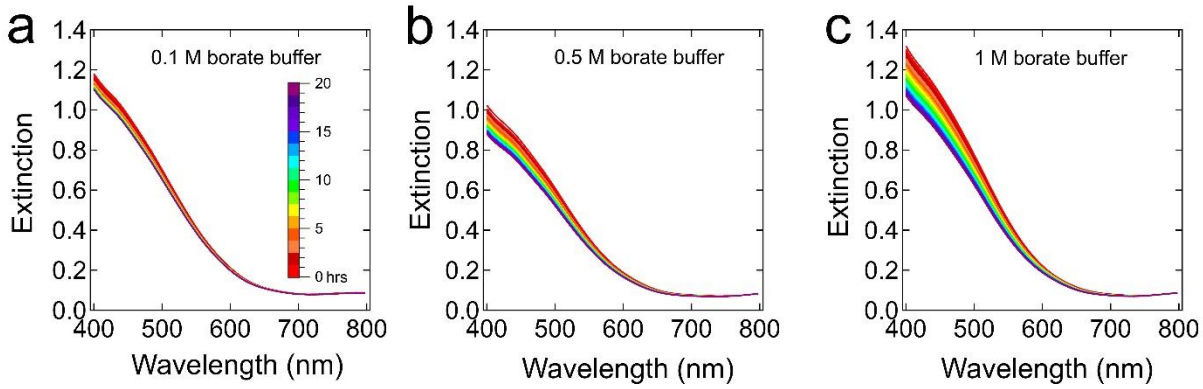

Figure S28. Effect of borate ion concentration on film stability. Spectral time series for a standard MVO film immersed in (a) 0.1 M, (b) 0.5 M and (c) 1 M borate buffer at pH 9 for 20 hours. [Mn] = [V] = 0.

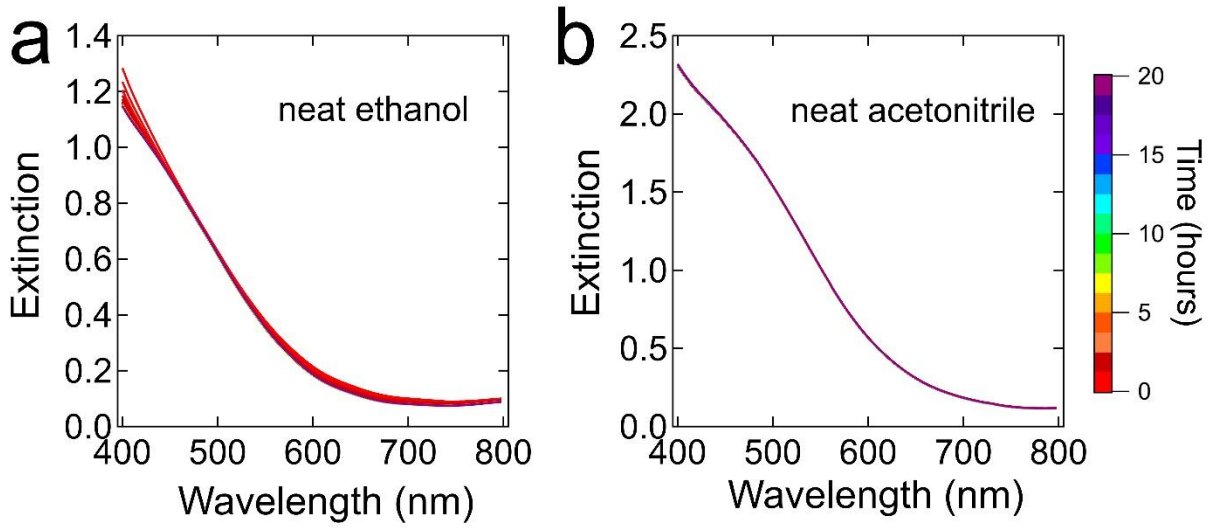

Figure S29. Film stability in pure ethanol and acetonitrile. Spectral time series for a standard MVO film immersed in (a) neat ethanol and (b) neat acetonitrile for 20 hours. [Mn] = [V] = 0.

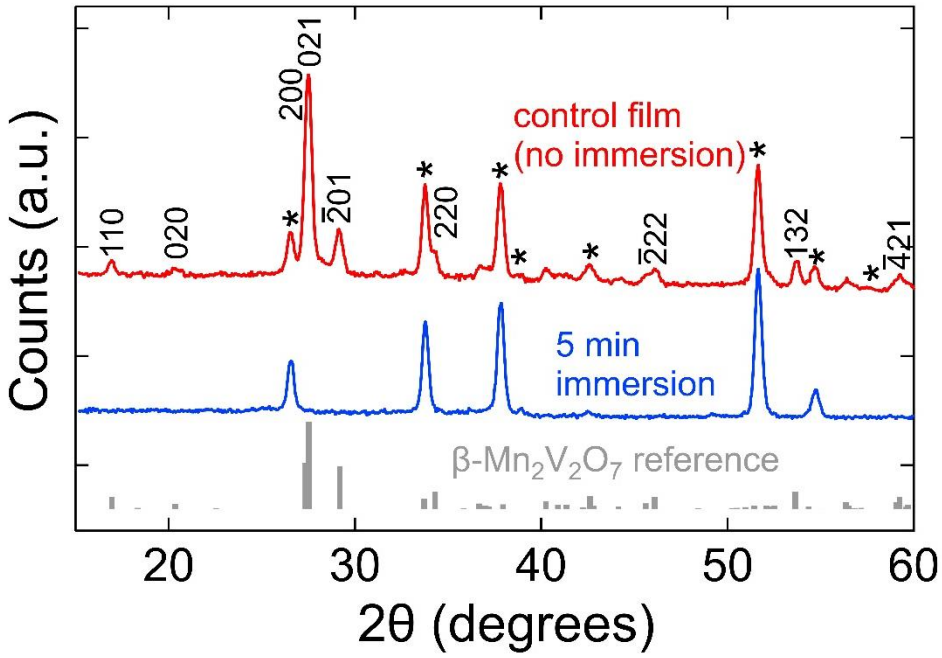

Figure S30. GIXRD pattern of a *β*-MVO film aged in pH 13 electrolyte for 5 minutes. The MVO peaks disappear. The angle of incidence was 0.79° for the aged film and 0.85° for the control film. The *β*-MVO reference pattern (gray bars) is also shown.

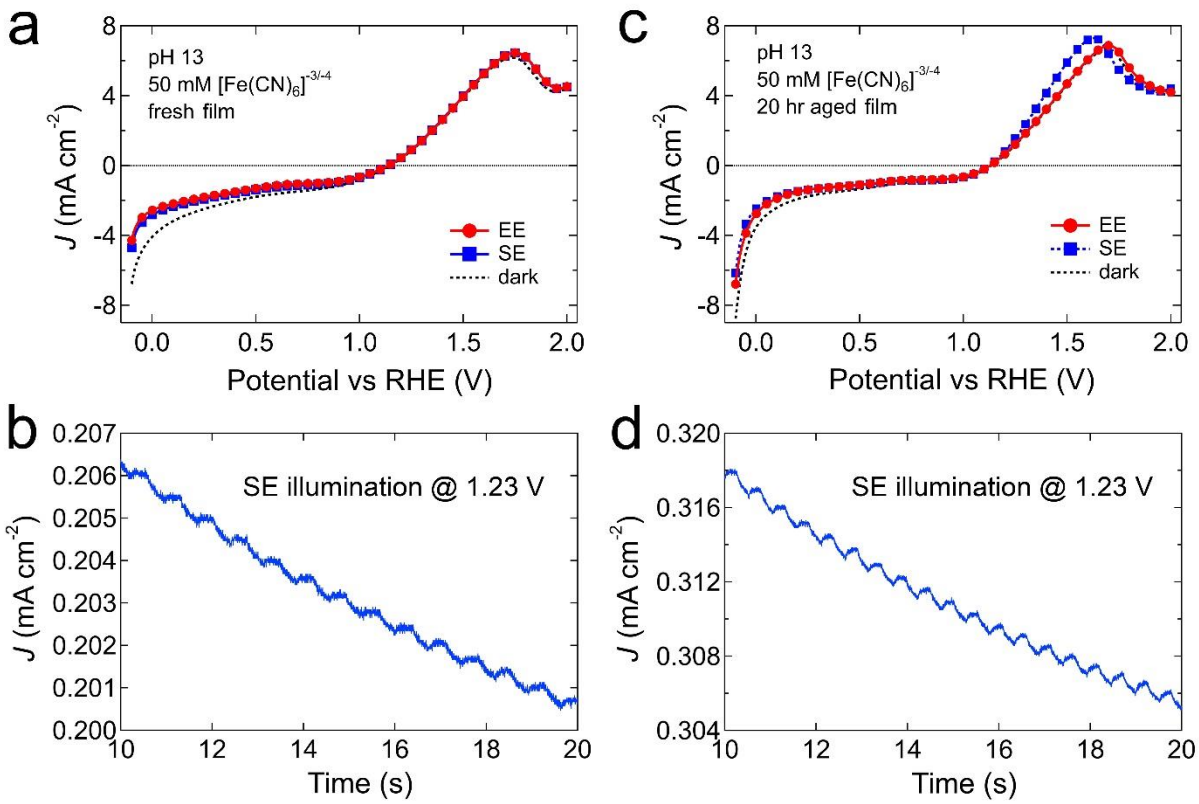

Figure S31. Representative photoelectrochemical data for MVO films in 0.1 M aqueous NaOH (pH 13) containing 50 mM $[Fe(CN)_6]^{3-/4-}$ redox couple. Current-potential (*J-E*) and current-time (*J-t*) plots for (a-b) a fresh film and (c-d) a film after 20 hours of immersion in the electrolyte (dark and unbiased). *J-E* data were acquired at a potential sweep rate of 50 mV/s. *J-t* data were acquired at 1.23 V vs. RHE using chopped illumination (1.25 Hz) in the SE geometry. Data acquisition for the fresh film started within 3-4 minutes of immersion in the electrolyte and required ~15 minutes to complete, during which time the film degraded significantly (see Fig. 5). The MVO films were 580 ± 60 nm thick. See Methods for other details.

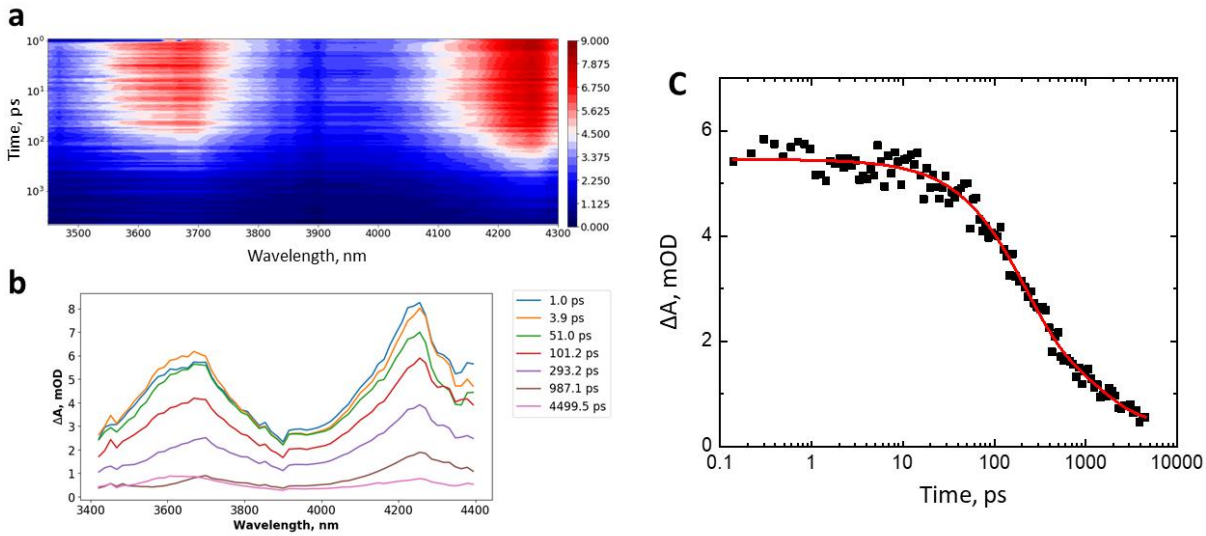

Figure S32. (a-b) Mid-IR transient absorption spectra and (c) kinetics for a dry MVO film pumped at 400 nm and probed at 4.2 μm. The spectral features are convoluted with the features of the mid-IR continuum probe.

Table S2. Fit parameters for mid-IR PIA kinetics.

	A_1	t_1 (ps)	A_2	t_2 (ps)
4200 nm decay	65%	197 (24)	35%	1389 (616)

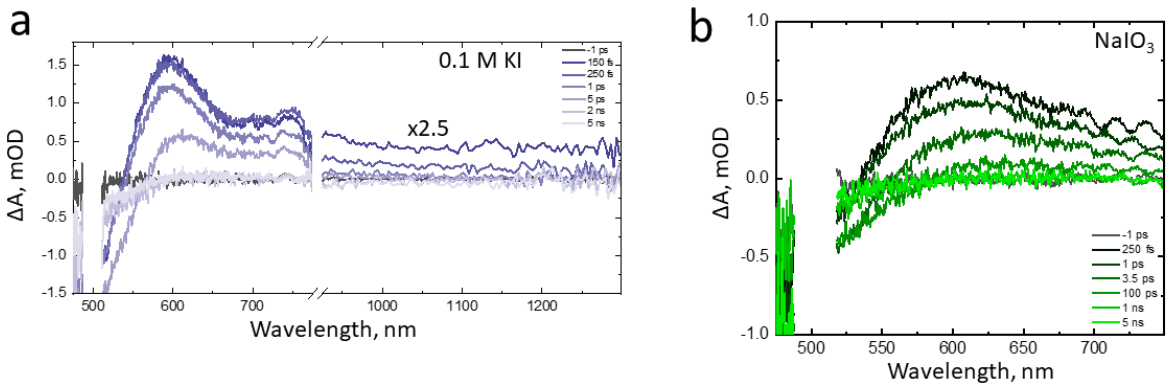

Figure S33. Transient absorption spectra at selected delay times for an MVO film immersed in (a) 0.1 M KI in 0.1 M borate buffer at pH 9 and (b) 0.1 M $NaIO_3$ in 0.1 M borate buffer at pH 9.

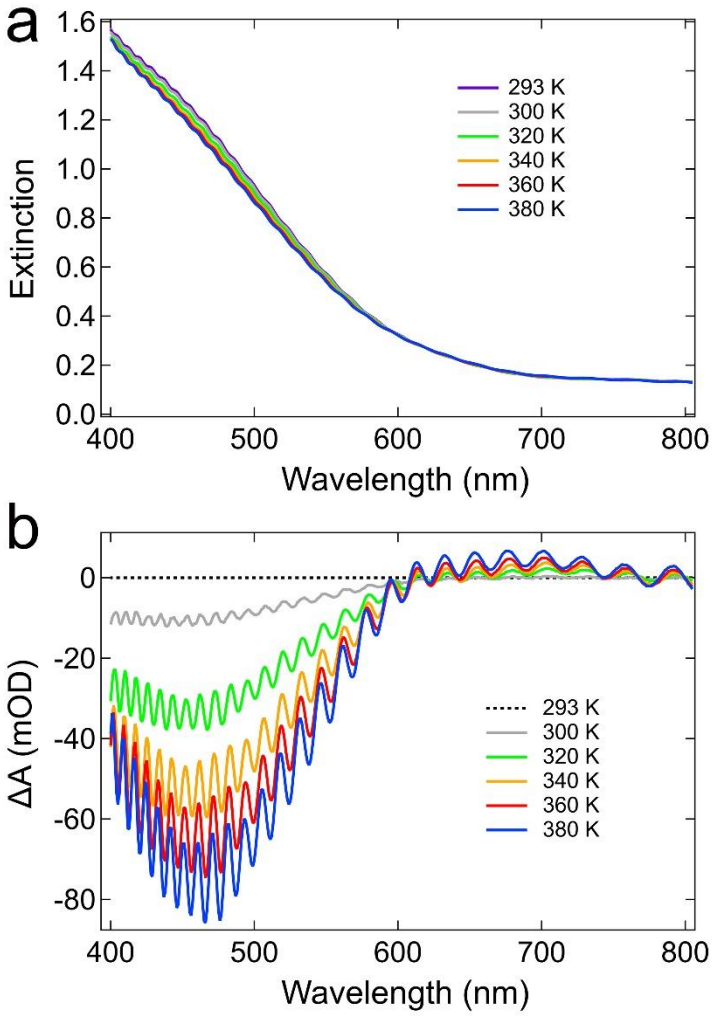

Figure S34. (a) Steady-state variable-temperature optical extinction spectra of a β-MVO film on a sapphire substrate from 293-380 K. (b) Corresponding difference spectra. Fringes in the spectra are due to Fabry-Perot interference.

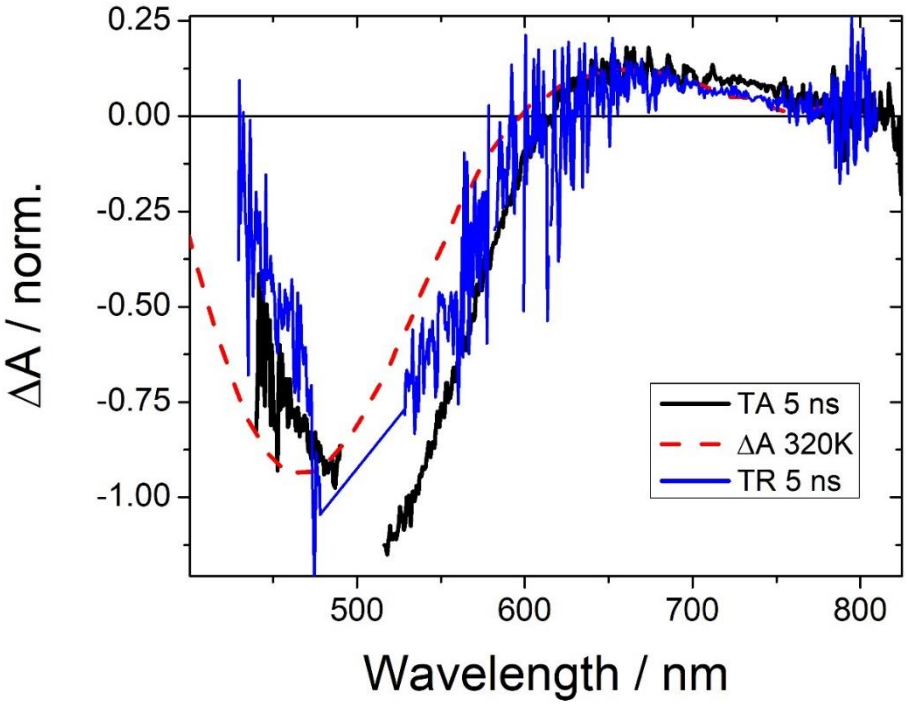

Figure S35. Comparison of the long-lived transient absorption (TA) spectrum (black), transient reflectivity (TR) spectrum (blue), and steady-steady extinction difference spectrum at 320 K (red) for a dry MVO film.

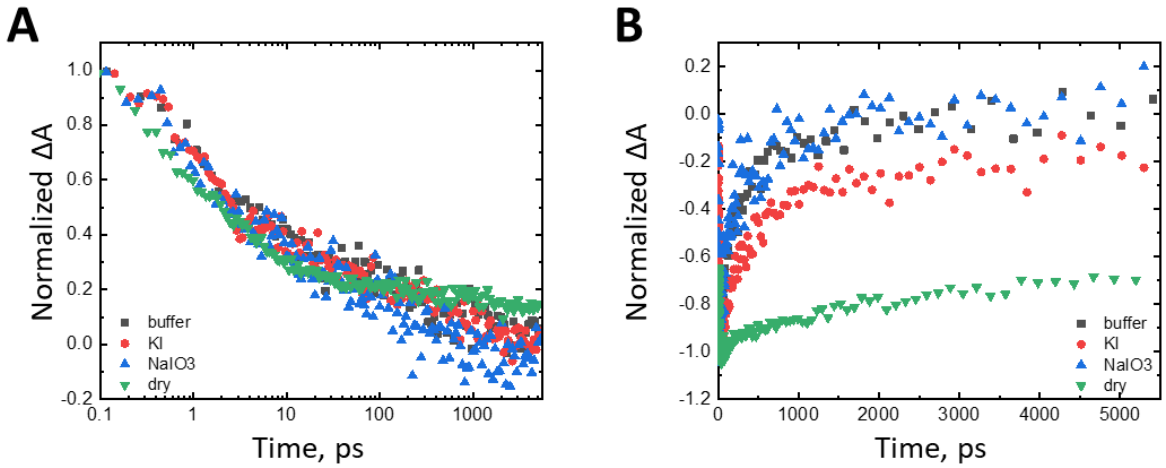

Figure S36. Kinetics of (a) the PIA at a 715 nm probe wavelength and (b) the GSB at 520 nm under various sample conditions.

Table S3. Fit parameters for PIA decay at 1100 nm.

	dry	0.1 M borate (pH 9)	buffer + 0.1 M KI
A_1	93%	87%	100%
t_1 (ps)	0.43 (0.03)	0.43 (0.03)	0.101 (0.02)
A_2	7%	13%	-
t_2 (ps)	176 (40)	377 (66)	-

References

(1) Gupta, R. P.; Sen, S. K. Calculation of Multiplet Structure of Core P-Vacancy Levels. *Phys. Rev. B* **1974**, *10*, 71–77.

(2) Nesbitt, H. W.; Banerjee, D. Interpretation of XPS Mn(2p) Spectra of Mn Oxyhydroxides and Constraints on the Mechanism of MnO 2 Precipitation. *A. Mineral.* **1998**, *83*, 305–315.

(3) Biesinger, M. C.; Payne, B. P.; Grosvenor, A. P.; Lau, L. W. M.; Gerson, A. R.; Smart, R. S. C. Resolving Surface Chemical States in XPS Analysis of First Row Transition Metals, Oxides and Hydroxides: Cr, Mn, Fe, Co and Ni. *Appl. Surf. Sci.* **2011**, *257*, 2717–2730.

(4) Ilton, E. S.; Post, J. E.; Heaney, P. J.; Ling, F. T.; Kerisit, S. N. XPS Determination of Mn Oxidation States in Mn (Hydr)Oxides. *Appl. Surf. Sci.* **2016**, *366*, 475–485.

(5) Ernens, D.; Langedijk, G.; Smit, P.; de Rooij, M. B.; Pasaribu, H. R.; Schipper, D. J. Characterization of the Adsorption Mechanism of Manganese Phosphate Conversion Coating Derived Tribofilms. *Tribol. Lett.* **2018**, *66*, 131.

(6) Franke, R.; Chassé, T.; Streubel, P.; Meisel, A. Auger Parameters and Relaxation Energies of Phosphorus in Solid Compounds. *J. Electron Spectros. Relat. Phenomena* **1991**, *56*, 381-388.